# NEUTRINO PROPAGATION IN DENSE ASTROPHYSICAL SYSTEMS

*Madappa Prakash and James M. Lattimer*

Department of Physics & Astronomy, State University of New York at Stony Brook

Stony Brook, NY 11794-3800, U.S.A.

*Raymond F. Sawyer*

Department of Physics, University of California at Santa Barbara

Santa Barbara, California 93106, U.S.A.

*Raymond R. Volkas*

School of Physics

Research Center for High Energy Physics, The University of Melbourne

Victoria 3010, Australia

KEYWORDS: Neutrinos in Dense Matter, Early Universe, Supernovae, Neutron Stars

**ABSTRACT:** Even the elusive neutrinos are trapped in matter, albeit transiently, in several astrophysical circumstances. Their interactions with the ambient matter not only reveal the properties of such exotic matter itself, but also shed light on the fundamental properties of the neutrinos themselves. The physical sites of interest include the early universe, supernovae,

and newly-born neutron stars. Detection of neutrinos from these vastly different eras using the new generation of neutrino detectors holds great promise for enhancing our understanding of neutrino-matter interactions and astrophysical phenomena.

CONTENTS



## 1 INTRODUCTION

In accelerator neutrino physics, a neutrino interacts once, with a constituent of the matter in a detector, to produce a signal. But in astrophysical situations

the surrounding matter can make a big difference to the neutrino physics. Some examples are:

(1) In their passage from the core of the sun to the solar surface, electron neutrinos ($\nu_e$) feel an "index of refraction", or altered energy-momentum connection, that is different from that for the other neutrino species, $\nu_\mu, \nu_\tau$. This difference is induced by forward scattering from electrons in the solar plasma. If there is in addition a "mass matrix" that would cause vacuum $\nu$ flavor oscillations, the changing index of refraction seen by a $\nu_e$ as it moves into regions of less density can give rise to the MSW effect. [1]

(2) The core of a collapsing star, and subsequently the interior of a newborn neutron star, or proto-neutron star (PNS), formed during the supernova process, is opaque to neutrinos. Initially, because neutrinos are trapped in the PNS, deleptonization of matter has yet to occur and the total number of leptons per baryon is about 0.4. Only after times of tens of seconds can neutrinos diffuse outwards and escape, but in so doing, they heat the matter through which they pass in a process reminiscent of Joule heating. Following this deleptonization is a cooling epoch, during which neutrinos continue to transport energy to the star's surface. The combination of extreme neutrino degeneracy and high temperatures and densities creates a unique environment in which the detailed neutrino processes and the resulting transport phenomena play an essential role. The escaping neutrino fluxes are crucial for the supernova dynamics, and are also important in the heavy element nucleosynthesis that might occur in the ejected envelope of the formerly collapsing star. Certainly, they determine the characteristics of the neutrino pulse that can be observed in terrestrial detectors (2).

[1] A recent review of neutrino oscillation physics is given in Ref. (1).

(3) In the standard model (three $\nu$ flavor) evolution of the early universe, in the temperature region of, roughly, $0.2 < k_B T/\mathrm{MeV} < 10$, the $\nu$'s and $\bar{\nu}$'s are very nearly in thermal equilibrium with the other particles in the plasma until the temperature drops below 1 MeV or so. The corrections to the distributions near this point of $\nu$ decoupling have been calculated quite well and provide a small change in the predictions of primordial $^4$He abundance. But there are models, involving flavor mixing and the possibility of a fourth neutrino flavor, in which the evolution of neutrino distributions, including the effects of interactions with the surrounding plasma, must be studied carefully at higher temperatures (see Section 4 below).

### *1.1 Orders of Magnitude*

We choose units so that $\hbar = c = k_B = 1$. Then the weak coupling constant is given by $G_F = 1.166 \times 10^{-11}$ (MeV)$^{-2}$. Number densities in these units for some systems of interest, are:

Solar center (electrons); $n_e \approx 6 \times 10^{25}$ cm$^{-3} \approx 5 \times 10^{-7}$ (MeV)$^3$

Earth core (electrons); $n_e \approx 5 \times 10^{-6}$ (MeV)$^3$

Supernova-core to neutrinosphere (nucleons) $n_N = [10^4 - 10^6]$ (MeV)$^3$

Early universe in the region, $1 < T/\mathrm{MeV} < 100$; $n_{\mathrm{particles}} \approx 5 \times T^3$.

We can estimate the length scales over which the effects of neutrino interactions with the media can be appreciable in the various cases:

(a) At solar center densities, the index of refraction correction from $\nu_e$-e forward scattering introduces a phase change of $2\pi$ in a distance

$\approx (n_e G_F)^{-1} \approx 4 \times 10^{18}$ (MeV)$^{-1} \approx 2 \times 10^7$ cm.

(b) The solar center mean free path for $\nu$ scattering is:

$\lambda_f \approx (n_e G_F^2 E_\nu^2)^{-1} \approx 2 \times 10^{28}$ (MeV)$^{-1} \approx 4 \times 10^{17}$(MeV/$E_\nu$)$^2$ cm.

This is far too long to be of any interest.

(c) The supernova center mean free path for neutrino scattering (but subject to substantial medium-dependent corrections to be discussed in this review) is

$\lambda_f \approx (n_N G_F^2 E_\nu^2)^{-1} \approx 2 \times 10^5$(MeV/$E_\nu$)$^2$ cm.

(d) For the early universe it is the neutrino collision time that is of interest

$\lambda_f/c \approx 10^{-21}/(G_F^2 T^5) \approx (T/\text{MeV})^{-3}$ s.

This, coupled to the expansion time, $t$(s)$\approx [T(\text{MeV})]^{-2}$, shows that $\nu$'s decouple from the medium at $T \approx 1$ MeV.

### *1.2 Scope of this Article*

In this review, we shall concentrate on the physics of neutrinos in supernovae, PNSs and in the early universe. For these problems one needs to follow the evolution of neutrino distributions in time. In all cases, we envision beginning with an initial condition with postulated or known neutrino distributions. In the early universe problem, the initial time can be taken to be sufficiently early for $\nu$ oscillations not to have affected the distributions; an initial temperature of tens of MeV suffices in the models that will be discussed.

In the supernova and PNS problems, we focus on the microphysics of neutrino interactions with matter. For the supernova case, neutrinos are initially freely streaming and act mainly as a cooling mechanism. Shortly after collapse begins, the neutrino mean free path becomes less than the size of the collapsing core, and neutrinos become trapped on dynamical time scales. During this period, there is a complex interaction between transport and hydrodynamics. While

we do not discuss supernova simulations in detail, we summarize the literature of recent results. For the PNS problem, which is quasi-hydrostatic, the initial distribution of neutrinos is that of a highly degenerate Fermi gas. We present results of transport simulations in PNSs for a variety of assumptions regarding the composition of matter.

In all three problems the dynamics of the system provides a time changing environment. And in these problems the particles other than $\nu$'s in the soup stay in near thermodynamic equilibrium. [2]

We attempt to pose cleanly some of the questions that have occupied theorists in these areas, to sketch somewhat qualitatively the methods that have been used, and to give some examples of results. A prototype neutrino evolution calculation involves three steps:

(1) deriving a kinetic equation that describes the macroscopic development of the evolution of the neutrino distribution;

(2) determining rate functions in the kernel of this equation that describe the local scattering, production and annihilation of the neutrinos; and

(3) solving the equation for a physical configuration.

Calculations of phenomena in this area are necessarily approximate but we shall attempt to define precisely the quantities that enter the equations. We must caution the reader that in most of the problems that we shall discuss there are, at present, few definitive results. In the first place, to the extent that neutrino mixing (or "oscillations") are involved, the mixing parameters are still undetermined. Furthermore, it is essential to follow the time development

[2] In the early universe, as we cool from, say, $T = 10$ MeV to 0.2 MeV the neutrons and protons go far out of chemical equilibrium, but the nucleons are far too sparse to affect the neutrino distributions significantly.

of non-equilibrium distributions of several species simultaneously. Finally, in the supernova and PNS applications, nuclear forces play an essential role in the opacities, and the macroscopic environment to be used in the supernova case is dependent on hydrodynamical calculations as well.

We warn the reader that the references are not exhaustive.

## 2 NEUTRINO MIXING AND INDEX OF REFRACTION EFFECT

The basis for what follows will be the standard model of neutrino interactions, in which all coupling is to the left handed neutrino current operators, in places supplemented by neutrino mass and mixing effects, or by the inclusion of a "sterile" neutrino, which has no interactions outside of the mixing term. If there is neutrino mass and mixing the standard model is augmented with a term of the form $H_{mix} = \sum_{\alpha,\beta} m_{\alpha,\beta}\bar{\psi}_\alpha\psi_\beta$, where the $\psi$'s are the $\nu$ fields and $(\alpha, \beta)$ are flavor indices, taking the values $e, \mu, \tau$ and, in the case of the consideration of a sterile neutrino, $s$.

The differences in the forward scattering amplitude of the different flavors of $\nu$'s in the various media, as calculated in first order in $G_F$, give rise to a relative energy shift matrix $\Delta_{\alpha,\beta}$ that is first order in $G_F$, independent of the neutrino energy, diagonal in the flavor indices, and proportional to the density of scatterers in the medium. In the usual MSW considerations this comes from the electron density, $n_e$, only and is given by $\Delta_{\alpha,\beta} = \delta_{\alpha,e}\delta_{\beta,e}\sqrt{2}G_F n_e$. However, in the interior of a supernova there may be enough $\mu^-$ present briefly to make a significant contribution to the forward scattering differences. Sterile neutrinos would add to the matrix, $\Delta$, as would one loop weak corrections under some

circumstances (3).

In all cases of interest, we have $m, \Delta \ll E_\nu$. Then standard Dirac technology combines the neutrino mass and index of refraction effects in an effective Hamiltonian for the $\nu, \bar{\nu}$ system, not including interactions, except for forward scattering,

$$H^{(\nu)} = \sum_{\mathbf{p},\alpha,\beta} \left\{ a^\dagger_\alpha(\mathbf{p}) a_\beta(\mathbf{p}) \left[ E\delta_{\alpha,\beta} + \lambda^{(+)}_{\alpha,\beta}(E) \right] + b^\dagger_\alpha(\mathbf{p}) b_\beta(\mathbf{p}) \left[ E\delta_{\alpha,\beta} + \lambda^{(-)}_{\alpha,\beta}(E) \right] \right\}, \quad (1)$$

where $E = |\mathbf{p}|$ and the $\lambda$ matrices are given by $\lambda^{(\pm)}(E) = m^2/(2E) \pm \Delta$. Here $a_\alpha(\mathbf{p})$ and $b_\alpha(\mathbf{p})$ are the respective annihilation operators for left-handed neutrinos and antineutrinos of flavor $\alpha$. The small admixtures of right handed $\nu$'s created by the mass term, for the case of Dirac neutrinos, are inconsequential in our applications. The magnitudes of the elements of the mass$^2$ matrix that have been suggested in the literature range from $10^{-15}(\mathrm{eV})^2$ to $1(\mathrm{eV})^2$ depending on the application.

## 3 KINETIC EQUATIONS

If there are no $\nu$ oscillations, the kinetic equations will be for distribution functions, $\rho_\alpha(\mathbf{p}, \mathbf{r}, \mathrm{t})$ for each flavor $\alpha$ of $\nu$ and $\bar{\nu}$, where the $r$ dependence is macroscopic in scale and originates from spatial variation of the properties of the medium, or in the initial condition taken for the neutrino distribution. For the case with neutrino oscillations, however, there can be off-diagonal flavor coherence that extends over large distances, and the system is no longer described in terms of a set of probabilities for the occupancy of the modes of the neutrino fields for each flavor. Instead we introduce a $\nu$ momentum-flavor density matrix, and discuss its evolution.

At $t = 0$ we take the density matrix for the complete system to be of the form of

a product of a neutrino matrix times an everything-else matrix, the everything-else being in thermal equilibrium; of course, these become entangled at later times. Introducing the operator, $\Lambda(\mathbf{k}, t=0)_{\alpha,\beta} = a^\dagger(\mathbf{k})_\alpha a(\mathbf{k})_\beta$, we define the momentum-flavor density matrix,

$$\rho_{\alpha,\beta}(\mathbf{k},t) = Z_{\neq\nu}^{-1}\ \mathrm{Tr}\Big[e^{-(H_{\neq\nu}-\sum_{i\neq\nu}\mu_i N_i)/T}\sum_i w_i \langle i\ ,\nu' s|\Lambda(\mathbf{k},t)_{\alpha,\beta}|i\ ,\nu' s\rangle\Big]\,, \quad (2)$$

where $\Lambda(\mathbf{k},t) = \exp(iHt)\Lambda(\mathbf{k},0)\exp(-iHt)$ , $H_{\neq\nu}$ is the Hamiltonian with all terms containing the $\nu$ coordinates left out, and $Z_{\neq\nu}$ is the partition function associated with this Hamiltonian. The states, $|i\ ,\nu' s\rangle$, represent all possible multi-$\nu$ states, indexed with $i$. The coefficients $w_i$ in the inner sum might be chosen in ways that are far from a thermal equilibrium configuration (for example, such that there are initially no sterile $\nu$'s, in models that contain a sterile $\nu$). $H$ is the complete Hamiltonian. We take the neutrino interaction with other particles to be of the form[3]

$$H_{int}^{(\nu)} = g\sum_{\alpha,\beta}\zeta_{\alpha,\beta}\bar{\psi}_\alpha[\gamma_\mu.....]\psi_\beta \times [\text{other fields}]\,, \quad (3)$$

where the matrix $\zeta$ acts in flavor space, and is generally diagonal in flavor. For example, if we are discussing active-sterile $\nu$ mixing we have, $\zeta_{a,a}=1$, $\zeta_{s,s} = \zeta_{a,s} = \zeta_{s,a} = 0$. For $\nu_e$ mixing with an active species, $a$, in an environment containing electrons and positrons but no other leptons, we have, $\zeta_{e,e} = 1 + c_e$, $\zeta_{a,a}=1$, where $c_e$ gives the effect of the charged current e, $\nu_e$ scattering term. There is no exact equation governing the time evolution of the function, $\rho_{\alpha,\beta}(\mathbf{k},t)$. Indeed, the evaluation of the two neutrino fields in $\Lambda(\mathbf{k})$ at the same momentum $\mathbf{k}$ rules out the derivation of such an equation. But if we had defined a density

[3]Generalizations to a sum of terms of this form are immediate, but give lengthier expressions in the evolution equations.

matrix with momentum indices, $\mathbf{k}, \mathbf{k}'$ then, at times large compared to a typical $E_\nu^{-1}$ we would find that, for all practical purposes, this density matrix was very nearly diagonal in these indices. We can qualitatively describe the simplification as due to the rapid decoherence between the parts of the $\nu$ wave function that are scattered at appreciably different momentum transfer (and/or energy transfer) from components of the medium at different (randomly situated) points in space, the density matrix in momentum space becoming nearly diagonal so fast that we need to consider only the diagonal elements in the $\mathbf{p}$ space. Finally, we consider only systems in which the local averages of the densities, compositions, and temperatures varies slowly in space, compared to all quantum mechanical distances except for the neutrino oscillation lengths. The evolution equation is then,

$$\frac{\partial}{\partial t}\rho(\mathbf{k},\mathbf{r},t) + |\mathbf{k}|^{-1}\mathbf{k}\cdot\nabla\rho(\mathbf{k},\mathbf{r},t) = -i[\lambda(E), P(\mathbf{k},\mathbf{r},t)] +$$
$$+\frac{1}{2}\sum_{\mathbf{k_1}}\Big[\zeta\rho(\mathbf{k_1},\mathbf{r},t)\zeta[1-\rho(\mathbf{k},\mathbf{r},t)] + [1-\rho(\mathbf{k},\mathbf{r},t)]\zeta\rho(\mathbf{k_1},\mathbf{r},t)\zeta\Big]\Gamma(\mathbf{k}_1,\mathbf{k})$$
$$-\frac{1}{2}\sum_{\mathbf{k_1}}\Big[\zeta[1-\rho(\mathbf{k_1},\mathbf{r},t)]\zeta\rho(\mathbf{k},\mathbf{r},t) + \rho(\mathbf{k},\mathbf{r},t)\zeta[1-\rho(\mathbf{k_1},\mathbf{r},t)]\zeta\Big]\Gamma(\mathbf{k},\mathbf{k}_1)\,. \qquad (4)$$

The function, $\Gamma(\mathbf{k},\mathbf{k_1})$, is the differential rate at which neutrinos would scatter from energy $\mathbf{k}$ to momentum $\mathbf{k_1}$ if we took $\zeta = 1$, that is, if the neutrino interaction were flavor independent. [4]

Many alternative paths to a derivation of equations like (4) are found in the literature. If we consider only the terms that are linear in $\rho$, as for the case

[4] As a concrete example, in the case in which one of the neutrinos is an electron neutrino, the plasma is constituted of electrons and positrons, and we consider $\nu_e$, $\nu_\mu$ mixing, $\Gamma$ stands for rate of scattering of $\nu_\mu$, and $\zeta$ is given as above. The squared amplitude contributions from scattering from electrons get added to those from positrons. So we can use $\zeta_{ee} = 1 + c$, just as though there were a single term in equation (3).

of a single neutrino traversing the medium, then with the right identifications equation (5) can be seen to be the same as the "quantum kinetic equation" of McKellar and Thomson (4), taken in the same limits. Using a somewhat idealized form of interaction, Raffelt, Sigl, and Stodolsky (5) have given an elegant derivation that includes Fermi statistics (i.e. the nonlinear terms on the RHS); they call the result the "non-Abelian Boltzmann equation." Again for the energy conserving case, but without Fermi statistics, Loreti and Balantekin (6) have used the equation, which they describe as a variant of the "Redfield equation" to analyze MSW transitions in media with irregular electron density variations in space. In the vast literature from the condensed matter and quantum optics side, such equations are often called "Bloch equations." Typical derivations are given in Refs. (7, 8). A simple derivation of equation (4) that captures most of the essential aspects of the physics, for the case of the density matrix of a single neutrino, is given in Ref. (9).

A simple application of equation (4) is to active-sterile mixing, involving two neutrino states that mix, only one of which scatters. For a translational and rotationally invariant system, we calculate a density matrix $\rho(E,t)$. We keep only the linear terms for illustration, and we adopt the representation $\rho = \frac{1}{2}(P_0 + \mathbf{P}\cdot\sigma)$, $\lambda = \mathbf{V}\cdot\sigma$ . The projection operator on the active state is $\zeta = (1+\sigma_z)/2$, where $\sigma$'s are the Pauli matrices. Substituting in equation (4) gives

$$\frac{\partial}{\partial t}\mathbf{P}(E,t) = \mathbf{V}(E)\times\mathbf{P}(E) - \frac{1}{2}\Big[\hat{x}P_x(E) + \hat{y}P_y(E)\Big]\sum_{E_1}\Gamma(E,E_1) + \hat{z}\frac{\partial}{\partial t}P_0(E,t) \quad (5)$$

and

$$\frac{\partial}{\partial t}P_0(E,t) = -\frac{1}{2}[P_z(E) + P_0(E)]\sum_{E_1}\Gamma(E,E_1) + \frac{1}{2}\sum_{E_1}\Gamma(E_1,E)[P_z(E_1) + P_0(E_1)]\,. \quad (6)$$

For later use in Section (4), it is helpful to define a decoherence function through $D \equiv (\Sigma_{E_1}\Gamma(E, E_1))/2$ and a repopulation function through $R \equiv \partial P_0/\partial t$.

### *3.1 Extensions of the Evolution Equation*

In the kinetic equation (4) the sources of change of the neutrino distribution are transport, flavor precession, and scattering. We sketch briefly the other effects that should be included. For economy in notation we can consider the spatially uniform case, in which the $\nu$ density matrix is given by $P_{\alpha,\beta}(E)$, as in equation (5).

**A. $\nu\bar{\nu}$ Pair Production and Annihilation:** These processes occur due to the conversion of charged lepton-anti-lepton pairs, or from $\nu$ pair bremsstrahlung processes. To include these, we can introduce a set of densities for antineutrinos and incorporate the coupling between the two sectors cominmg from pair processes. However, it is neater, to define the function $[1 - \rho(-E)]$ as the $\bar{\nu}$ density matrix, to use the extension of $\lambda(E)$ to negative energies provided by the definition in equation (2), and to extend the functions, $\Gamma(E, E_1)$, so that for $E < 0, E_1 > 0$ it is the pair production rate, for $E > 0, E_1 < 0$ the pair annihilation rate, and for $E < 0, E_1 < 0$ the anti-particle scattering rate, but from energy, $-E_1$, to energy $-E$. With these conventions the only change to be made in equation (5), to accomodate pair creation and annihilation will be to relabel the energy sums in equation (5) to be $\sum_{E_1=-\infty}^{\infty}$. In the case $\lambda = 0$, $\zeta = 1$, the system would move toward a thermal equilibrium described by a $\nu, \bar{\nu}$ Fermi distributions with a single chemical potential determined by the excess lepton number for each flavor.

**B. Expansion of the Universe:** This is taken into account by using the time dependent temperature in the statistical factor and adding to the LHS of equation (5) the term $-[\dot{a}(t)/a(t)]E(\partial/\partial E)\rho(E,t)$ where $a(t)$ is the scale factor.

**C. Charged-Current Interactions of Electrons with Nucleons:** This requires an additional term on the RHS of equation (5), of the form, $-\delta_{\alpha,e}\delta_{\beta,e}[\rho_{\alpha,\beta}(E)\Gamma_a(E) + (1-\rho_{\alpha,\beta})\Gamma_e(E)]$, where $\Gamma_a$ and $\Gamma_e$ are the appropriate differential rates for absorption and emission, from the medium, of a $\nu_e$.

**D. Neutrino-Neutrino Scattering:** At the present stage of the development of the formalism the effects of $\nu - \nu$ scattering must be put in by hand in a way that suits the application.

In modern supernova calculations in the absence of neutrino mixing, it is usual to bypass the explicit Boltzmann equation for the evolution of the density functions, and to do neutrino transport by following the neutrino distributions numerically, energy bin by energy bin, and region by region in space. The basic input is the differential rate function, $\Gamma(E, E_1)$ introduced above. Much of the review to follow will be concerned with the calculation of these functions in the presence of strong interactions among the constituents of the matter.

However, we note that the equation governing the evolution of the distribution function in the presence of mixing cannot be interpreted as assigning probabilities, effective immediately, at the outcome of every neutrino interaction. It is clear that the numerical simulation of a case with neutrino mixing, involving some phase information that may propagate through many scattering interactions, will be more complex, and will require going back to the equation for the distribution function that is shown above.

### *3.2 Determination of the Rate Functions*

In applications we need only terms of order $G_F^2$. The rates, in media that are in thermal equilibrium are given by thermal averages of Heisenberg picture current operators. For neutral current scattering we define a current correlator, $W_{\mu\nu}$,

$$W_{\mu\nu}(q,\omega) = Z^{-1} \int d^4x \; e^{-i\mathbf{q}\cdot\mathbf{x}} e^{i\omega t} \; \mathrm{Tr}[e^{-\beta(H-\Sigma\mu_i N_i)} j_\mu(\mathbf{x},t) j_\nu(0,0)] \,, \qquad (7)$$

where the $j_\mu$ is the neutral current operator, which we have taken to be independent of $\nu$ flavor .[5] The quantities $H$ and $N_i$ contain only the coordinates of the species that are in equilibrium. The differential rate for neutrino scattering, at angle $\theta$ and with energy loss of $\omega$, or gain of $(-\omega)$, is

$$\frac{d^2\Gamma}{d\omega \, d\cos\theta} = (4\pi^2)^{-1} G_F^2 (E_1-\omega)^2 [1 - f_\nu(E_1-\omega)] \Lambda^{\mu\nu}(q,\omega) W_{\mu\nu}(q,\omega) \,, \qquad (8)$$

where $\mathbf{q} = \mathbf{p_1} - \mathbf{p_2}$ is the momentum transferred from the neutrino to the medium, $Z$ is the partition function, and

$$\Lambda^{\mu\nu} = (4E_1E_2)^{-1} \; \mathrm{Tr}[\not{p}_1 \; (1-\gamma_5)\gamma^\mu \not{p}_2 \; \gamma^\nu (1-\gamma_5)]. \qquad (9)$$

For the case of charged current reactions there is a parallel construction, where we now take $j_\mu$ to be the hadronic current that is coupled to electron emission, with its Hermitean conjugate the current that is coupled to electron absorption:

$$W^{(ch)}_{\mu,\nu}(q,\omega) = -iZ^{-1} \int d^4x \; e^{-i\mathbf{q}\cdot\mathbf{x}} e^{i(\omega+\hat{\mu})t} \; \mathrm{Tr}[e^{-\beta(H-\Sigma\mu_i N_i)} j_\mu(\mathbf{x},t) j^\dagger_\nu(0,0)] \,, \quad (10)$$

where $\hat{\mu}$ is the chemical potential difference $\hat{\mu} = \mu_n - \mu_p$. In the early universe application, where the medium is comprised almost entirely of $\mathrm{e}^\pm$, $\nu, \bar{\nu}$, it is quite a good approximation to replace the formal expressions for the functions

[5] In applications in which $(\nu_e, e)$ scattering plays a role, it is convenient to include the charged current contribution to the $(\nu_e, e)$ interaction in this term, giving a dependence on the $\nu$ flavor indices that we do not show explicitly.

that determine the rates, such as $W_{\mu\nu}$ in equation (8), by their vacuum Born approximations, modified only by the statistical factors for the external particles. But there are corrections of order 1% in the predicted $^4$He abundance that come from careful nonequilibrium calculation of the functions related to $W_{\mu\nu}$ in the thermal environment (10, 11).

In the supernova environment, however, the densities and temperatures from the core to the neutrinosphere, at the average radius of the last $\nu$ scattering, are such that the wavelength of a thermal neutrino is greater than the interparticle spacing, so that neutrino scattering is a collective phenomenon. In this case a treatment must begin directly from the dynamical functions defined in equations (7) and (10) rather than from the (cross section×density) expression that applies to dilute systems or for more energetic neutrinos. In the center of the region the densities are on the order of nuclear densities ($n_o \simeq 0.16$ fm$^{-3}$) and the matter is quite degenerate, much like the nuclear matter that has been discussed with respect to the interiors of heavy nuclei or neutron stars. But nearly all the way to the $\nu$-sphere, at a density $\approx 0.01 n_0$ and with $T \approx$5 MeV, strong interactions among the nucleons will significantly affect the rates of neutrino processes, due to the fact that $T$ is less than the per-nucleon interaction energy throughout most of the region.

### 3.2.1 Long-Wavelength Limits

The results of the detailed calculations that will be summarized below indicate that the main features of the combined effects of Fermi statistics and of the nuclear interactions can be described by some simple limits. When the neutrino has energy of the order $T \ll M_N$ there is relatively small energy transferable

to the nucleons. Then integrating equation (8) over $\omega$ to get the rate that is differential in angle only, the correlator $W_{\mu\nu}(\mathbf{q},\omega)$ has a peak around $\omega = 0$ and the multiplying factors can be evaluated at $\omega = 0$. Thus what enters the total rate is the the energy integral of the correlator itself, or the $t = 0$ value of the time dependent correlator. As illustration we take the vector current only, with a coupling to a single kind of nucleon, and define a structure factor, $S(q)$, by

$$nS(q) = (2\pi)^{-1} \int_{-\infty}^{\infty} d\omega \; W_{00}(q,\omega)\,. \tag{11}$$

Looking first at a free nearly-degenerate Fermi gas, $T \ll E_F$, we find that $S(q)$ is less than unity because of the Pauli principle reduction of phase space. There is some phase space available for two reasons:

(a) The Fermi surface is diffuse, since $T \neq 0$, with some states below the Fermi energy unoccupied, and some above occupied. No matter how small the momentum transfers, this gives some room for transitions, with a rate contribution proportional to $T$.

(b) There is also a $T = 0$ limit, but here the neutrino scattering, with momentum transfer $q$, must excite a state from below to above the Fermi level.

At low temperatures these corrections are additive. But when $q \approx T$ the (a) terms, proportional to $T$, will always predominate over the (b) terms, by the ratio of the speed of light to the Fermi velocity (12). (The nucleons are quite non-relativistic in most cases.)

Turning to the case with nucleon-nucleon interactions, again for thermal q, so that the terms proportional to $T$ dominate, we can use a powerful classical result: in our one species gas the long wavelength limit of the structure factor is given by

$$\mathrm{Lim}_{q\to 0} \; S(q) = nT\kappa_T^{-1}\,. \tag{12}$$

Here $\kappa_T$ is the isothermal bulk modulus, $\kappa_T = n[\partial P/\partial n]_T = n\partial^2 F/\partial n^2$, where $P$ is the pressure and $F$ is the Helmholtz free energy density. Note that if the equation of state (EOS) were that of a free Boltzmann gas $P = nT$, equation (12) gives the uncorrelated value $S = 1$. If the EOS is that of a degenerate Fermi gas, then we get the same answer as in the dominating term proportional to $T$ in the direct Pauli blocking calculation reviewed above. Using equation (12) we have replaced a correlation function calculation by an EOS calculation. This pays dividends for the case of the strongly interacting gas. For example, in the nearly degenerate case we get the dominating term in the structure function, proportional to $T$, from the zero-temperature EOS, for which nuclear matter calculations provide data. We also get a qualitative lesson directly from equation (12), namely that attractive interactions, which soften the equation of state (reduce $\kappa_T$), increase neutrino scattering while repulsive interactions decrease neutrino scattering.

For the neutrino scattering case, the axial current (Gamow-Teller or GT for short) terms coming from equation (7) depend on the nucleon spin density correlators, rather then the density correlators. These terms provide roughly 3/4 of the scattering, in the free particles case. It is straightforward to generalize the above small $q$ analysis. The results are that the GT terms in the total opacity have a structure similar to equation (12), but with $\kappa_T$ in the denominator replaced by $\kappa_{\rm spin} = n_s\partial^2 F/\partial n_s^2$, where $n_s$ is the spin density of the system. That is to say, in order to determine the spin density correlators that determine the rate functions we must calculate the free energy (or energy, in the case of the nearly degenerate system) with a constraint of non-vanishing expectation of nuclear spin, to second order in the spin excess. This would seem to be within the range of variational nuclear matter calculations (13), but it has not been carried through for the phe-

nomenological potentials that are in use. For the case of the nuclear matter in nuclei however, to the extent that the term "nuclear matter" is applicable, it is the modulus $\kappa_{\rm spin}$ that determines the parameters of the giant GT resonances, so that there is indeed the possibility of using values determined fairly directly from data rather than those coming from nuclear matter calculations based on a specific potential.

### 3.2.2 Strong and Electromagnetic Correlations

With these remarks as orientation, we describe the ring graph calculation of the correlators. Although we will quote results from more than one source, and more than one exact set of assumptions, the basic inputs are Fermi liquid parameters that incorporate a good deal of nuclear phenomenology. These parameters are effectively the coupling constants of zero range N-N potentials that describe the low energy excitations of the matter. The ring graph sum has two properties that are important to us in the light of the above discussion:

(1) In the $q = 0$ limit, the sum of the ring graphs for the correlators gives back the connection equation (12) when we take the system's free energy density to be given by its Hartree value. There is a similar connection for the spin response part.

(2) In contrast to the model of a free nucleon gas, in which the neutrino-nucleon collisions are nearly elastic, the ring results show that significant gains and losses of neutrino energy may be realized in the collision. Much of this inelasticity is found to be in the form of the emission and absorption of spin waves in the medium: these are the continuous matter analogues of the giant GT resonances in nuclei. The giant GT resonance was a principal ingredient in the

phenomenological determination of the "spin-isospin" Fermi liquid parameter that goes into our model. The dispersion relation that describes the nuclear GT resonances (with "momentum" $\approx \pi$/nuclear radius) is consistent with the Cerenkov angle found in (14–18) for the emission of a spin wave into the medium. Whatever residual deficiencies there may be in the method, or in our underlying simplification of the nuclear interactions, what follows captures some of the essential physics. The ring equations, which we shall give in rather schematic form, begin with the definition of a "polarization" $\Pi_{\mu\nu}$ through the following replacements on the LHS and RHS of equation (8) $W_{\mu\nu}(\mathbf{q},\omega) \rightarrow \Pi_{\mu\nu}(\mathbf{q},\omega)$ and $j_\mu(\mathbf{x},t)j_\nu(0,0) \rightarrow [j_\mu(\mathbf{x},t), j_\nu(0,0)]\theta(t)$, the retarded commutator being the structure of choice for many-body graph summing. Then the rate function $W_{\mu\nu}$ is recaptured through,

$$W_{\mu\nu}(q,\omega) = 2(1-e^{-\beta\omega})^{-1}\mathrm{Im}[\Pi_{\mu\nu}(q,\omega)]. \tag{13}$$

The function $\Pi_{\mu\nu}(q,\omega)$ can be decomposed in scalar functions. For simplicity we illustrate the ring approximation (sometimes referred to as the RPA) for the case of the vector current part of the neutral current coupling to a single species of nucleon (or, equivalently, to the isoscalar part of the coupling to protons and neutrons). In this case the time components $\Pi_{00}(q,\omega) \equiv \Pi(q,\omega)$ obey the ring equation,

$$\Pi(q,\omega) = \frac{\Pi^{(0)}(q,\omega)}{1-v(q)\Pi^{(0)}(q,\omega)}\,, \tag{14}$$

where $v(q) = \int d^3x\ \exp[i\mathbf{q}\cdot\mathbf{x}]V(x)$ and $\Pi^{(0)}(q,\omega)$ is the free polarization part. If we take only the numerator in equation (14), we recover the effects of Pauli blocking alone.

This approach can be fleshed out to include spin and isospin, giving rise to multichannel equations; then the minimal $v(q)$ in equation (14), now a matrix in

channel space, can be taken from the Fermi liquid parameters as estimated, e.g., in (19). Details and further discussion of these methods can be found in Refs. (14–18).

The extension of these methods to encompass a relativistic field-theoretic description of the matter in which the neutrinos propogate is straightforward (16, 17, 20); in this approach the target particle time ordered or causal polarization tensor is calculated using

$$\Pi_{\mu\nu} = -i \int \frac{d^4p}{(2\pi)^4} \mathrm{Tr}\, \left[ T(G_2(p) J_\mu G_4(p+q) J_\nu) \right] . \tag{15}$$

The Greens' functions $G_i(p)$ (the index $i$ labels particle species) describe the propagation of baryons at finite density and temperature. The current operator $J_\mu$ is $\gamma_\mu$ for the vector current and $\gamma_\mu\gamma_5$ for the axial current. Effects of strong and electromagnetic correlations may be calculated by utilizing the RPA polarization tensor

$$\Pi^{RPA} = \Pi + \Pi^{RPA} D \Pi \ , \tag{16}$$

where $D$ denotes the interaction matrix (see (17, 20) for more details).

### 3.2.3 Neutrino Scattering in Heterogeneous Media

The coherent scattering of neutrinos from heterogeneous media was first discussed by Freedman (21) in conjunction with heavy nuclei in the subnuclear density regime. For neutrino de Broglie wavelengths $\lambda_\nu >> R_N$, where $R_N$ is nuclear radius, the opacity is enhanced by a factor $N^2/6A \approx 100$ compared to that from the same mass density of nucleons alone (21). In the supernova environment, coherent scattering dominates all other opacity sources. However, nuclei are relatively close together and the neutrino wavelengths are not necessarily large. Three important corrections (22) that must be applied which reduce

the coherent cross section include the nuclear structure factor (when $\lambda_\nu < R_N$), liquid structure effects (when $\lambda_\nu > R_N\ (n_0/n)^{1/3}$, the internuclear spacing), and polarization of the medium by the electrons (when $\lambda_\nu > R_D$, where $R_D$ is the Debye radius). Obviously, effects that influence the nuclear radius, such as the internuclear spacing, the nuclear surface energy, and finite temperatures, are very important, and are equation of state sensitive. In addition, around $n_0/3$, where the nuclear phase might transform into an inside-out, or bubble, phase, structural effects could play a role in neutrino cross sections.

More recently, coherent scattering from droplets of exotic matter (kaon condensates or quark matter) in the supranuclear density regime has been also considered (23) for the PNS environment.

The Lagrangian that describes the neutral current coupling of neutrinos to the droplet (either a nucleus or a droplet of exotic matter) is

$$\mathcal{L}_W = \frac{G_F}{2\sqrt{2}}\ \bar{\nu}\gamma_\mu(1-\gamma_5)\nu\ J_D^\mu\,, \tag{17}$$

where $J_D^\mu$ is the neutral current carried by the droplet. For non-relativistic droplets, $J_D^\mu = \rho_W(x)\ \delta^{\mu 0}$ has only a time like component. Here, $\rho_W(x)$ is the excess weak charge density in the droplet. The total weak charge enclosed in a droplet of radius $R_N$ is $N_W = \int_0^{R_N} d^3x\ \rho_W(x)$ and the form factor is $F(q) = (1/N_W)\int_0^{R_N} d^3x\ \rho_W(x)\ \sin qx/qx$. The differential cross section for neutrinos scattering from an isolated droplet is then

$$\frac{d\sigma}{d\cos\theta} = \frac{E_\nu^2}{16\pi} G_F^2 N_W^2 (1+\cos\theta) F^2(q)\,, \tag{18}$$

where $E_\nu$ is the neutrino energy, $\theta$ is the scattering angle, and $q = \sqrt{2}E_\nu(1-\cos\theta)$ is the momentum transfer. Since the droplets are massive, elastic scattering dominates.

The droplet radius $R_N$ and the inter-droplet spacing are determined by the balance between surface and Coulomb energies. In the Wigner-Seitz approximation, the cell radius is $R_W = (3/4\pi N_D)^{1/3}$, where the droplet density is $N_D$. Except for one aspect, we will neglect coherent scattering from more than one droplet. If the droplets form a lattice, Bragg scattering will dominate and our description would not be valid. But for low density and a liquid phase, interference from multiple droplets affects scattering only at long wavelengths. If the temperature is not small compared to the melting temperature, the droplet phase will be a liquid and interference from scattering off different droplets are small for neutrino energies $E_\nu \gtrsim (1/R_W)$. However, multiple droplet scattering cannot be neglected for $E_\nu \lesssim 1/R_W$. The effects of other droplets is to cancel scattering in the forward direction, because the interference is destructive except at exactly zero degrees, where it produces a change in the index of refraction of the medium. These effects are usually incorporated by multiplying the differential cross section equation (18) by the static form factor of the medium

$$S(q) = 1 + N_D \int d^3r \exp i\mathbf{q}.\mathbf{r}\ (g(r) - 1)\,, \tag{19}$$

where $g(r)$ is the radial distribution function of the droplets. The droplet correlations, which determine $g(r)$, are measured in terms of the dimensionless Coulomb number $\Gamma = Z^2e^2/(8\pi R_W kT)$. Due to the long-range character of the Coulomb force, the role of screening and the finite droplet size, $g(r)$ cannot be computed analytically. We use a simple ansatz for the radial distribution function $g(r < R_W) = 0$ and $g(r > R_W) = 1$. For this choice, $S(q)$ is independent of $\Gamma$. Monte Carlo calculations (24) of a simple one component plasma indicate that this choice of $S(q)$ is adequate for neutrino energies of interest.

The simple ansatz for $g(r)$ is equivalent to subtracting, from the weak charge

density $\rho_W$, a uniform density which has the same total weak charge $N_W$ as the matter in the Wigner-Seitz cell. Thus, effects due to $S(q)$ may be incorporated by replacing the form factor $F(q)$ by

$$F(q) \rightarrow \tilde{F}(q) = F(q) - 3\,\frac{\sin qR_W - (qR_W)\cos qR_W}{(qR_W)^3}\,. \tag{20}$$

The neutrino–droplet differential cross section per unit volume is then

$$\frac{1}{V}\frac{d\sigma}{d\cos\theta} = N_D\,\frac{E_\nu^2}{16\pi}G_F^2 N_W^2(1+\cos\theta)\tilde{F}^2(q)\,. \tag{21}$$

Note that even for small $N_D$, the factor $N_W^2$, which in the case of nuclei is proportional to $N$, serves to enhance the droplet scattering.

This concludes our overview of some of the technical tools that are needed and available to address media-related issues.

### *3.3 Neutrino Mean Free Paths: Examples*

The differential cross section in equation (8) is required in multi-energy group neutrino transport calculations (see Section 5.1). However, more approximate neutrino transport schemes (such as those described in Section 5.2.2) utilize the total cross section per unit volume (or equivalently the inverse mean free path), integrated over the angle $\theta$ and energy transfer $\omega$ in equation (8), as a function of the neutrino energy. Examples of such neutrino scattering (that is common to all neutrino species) and absorption mean free paths for conditions relevant to the deleptonization and cooling epochs of PNSs are considered below. The equations of state used in these calculations are described in (25).

**A. Effects of Composition:** Under degenerate conditions even modest changes to the composition significantly alter the neutrino mean free paths. In Figure 1 the top (bottom) panels show the scattering (scattering plus absorption) mean

free paths in neutrino-free (neutrino-trapped) matter. The left (right) panels show results for selected temperatures (for the neutrino energy $E_\nu = \pi T$) in matter without (with) hyperons. The presence of hyperons significantly decreases the mean free paths in both environments because of the additional available channels.

During the deleptonization stage, charged current reactions in fact dominate scattering reactions. At zero temperature, reactions like the direct Urca process $\nu + n \leftrightarrow e + p$ depend sensitively on the proton fraction $Y_p$ (26). Kinematic restrictions require $Y_p$ to be larger than $11 - 14\%$ (this is called the direct Urca threshold). At early times, when large numbers of trapped neutrinos are present, these reactions proceed without hindrance. After several tens of seconds, however, $Y_p$, which depends sensitively on the density dependence of the nuclear symmetry energy, decreases to its cold, catalyzed value. In field-theoretical models, the symmetry energy is largely controled by the $\rho$-meson exchange which increases strongly with density, and establishes a typical critical density $n_c = 2 \sim 3n_0$. However, at finite temperature, the equilbrium $Y_p$ and average $E_\nu$ values are larger than at zero temperature, enabling the charged current reactions to proceed even below $n_c$. Figure 2 shows that this is indeed the case even at relatively low temperatures ($T \sim 3 - 5$) MeV for a baryon density $n_B = 0.15$ fm$^{-3}$. Thus, Urca processes dominate the opacity until very late times.

**B. Effects of Strong and Electromagnetic Correlations:** The RPA and Hartree scattering mean free paths of thermal neutrinos in neutrino-free matter are compared in Figure 3. Correlations are generally more important with increasing density and decreasing temperature. The density dependence is chiefly

due to variations in the effective baryon mass, which is controlled by the Fermi Liquid parameter $g'$. The RPA correlations, even for a large $g'$, will typically increase the mean free path by a factor $2 - 2.5$.

The RPA and Hartree absorption mean free paths are compared in Figure 4 for neutrino-trapped matter. The qualitative trends for neutrino-free matter are similar, although the largest enhancements due to correlations are a factor of 5 in the neutrino-free case instead of about 2 in the neutrino-trapped case. In both cases, the results are quite similar to those for the scattering case shown in Figure 3.

**C. Mean Free Paths in Quark Matter:** An intriguing possibility is that sufficiently dense matter contains deconfined quarks. It is likely that quark matter, if it exists, will comprise one component of a mixed phase with hadrons (27). Within the mixed phase, the thermodynamic and chemical potentials will be rather different than in ordinary hadronic matter of the same density. As a result, significant effects on neutrino opacities are anticipated. Figure 5 shows scattering and absorption mean free paths, for the cases of matter with trapped neutrinos and neutrino-free matter, in which a mixed phase occurs (28). The vertical dashed lines indicate the central densities of 1.4 $M_\odot$ stars and maximum mass stars, respectively; densities above the right-most vertical line cannot be achieved in any neutron star. The thin curves show the mean free paths for the respective matter (hadrons or quarks) in their pure phases, while their values within the mixed phase are indicated by thick curves. The chief consequence of a mixed phase is that it reverses the trend of pure hadronic matter to have steadily decreasing mean free paths with increasing densities. In other words,

matter within the mixed phase region is substantially more transparent than matter without such a transition, whether or not the matter is composed of pure hadrons or quarks. Partly, this result is a consequence of the fact that the entropy is held fixed in these panels: quark matter has a higher specific heat than hadronic matter and favors a lower temperature. In the presence of a mixed phase, the temperature is smaller than in its absence, and the neutrino cross sections, which increase roughly as $T^2$, decrease.

**D. Droplet Scattering In Heterogeneous Phases:** Models of first order phase transitions in dense matter (29) provide the weak charge and form factors of the droplets and permit the evaluation of $\nu$–droplet scattering contributions to the opacity of the mixed phase (23). For first order kaon condensate and quark-hadron phase transitions, the neutrino mean free paths in the mixed phase are shown in the left and right panels of Figure 6, respectively. The transport cross sections in diffusive transport are usually differential cross sections weighted by the angular factor $(1-\cos\theta)$. The kaon droplets are characterized by radii $R_N \sim 7$ fm and inter-droplet spacings $R_W \sim 20$ fm, and enclose a net weak vector charge $N_W \sim 700$. The quark droplets are characterized by $R_N \sim 5$ fm and $R_W \sim 11$ fm, and an enclosed weak charge $N_W \sim 850$. For comparison, the neutrino mean free paths in uniform neutron matter at the same density and temperature are also shown. A large magnification in the opacity exists for $E_\nu \sim \pi T$. At much lower energies, the inter-droplet correlations tend to screen the weak charge of the droplet, and at higher energies the coherence is attenuated by the droplet form factor. Similar effects occur in the case of coherent scattering from nuclei (22).

# 4 NEUTRINOS IN THE EARLY UNIVERSE

## *4.1 Big Bang Nucleosynthesis*

An interesting application of neutrino transport in a dense medium lies in the study of neutrino oscillations in that phase of the early universe immediately prior to and during Big Bang Nucleosynthesis (BBN) (30). Neutrinos play two very important roles during BBN.

First, light neutrinos will be relativistic during the nucleosynthetic epoch, and so contribute to driving the expansion of the universe. Under radiation dominance, the expansion rate or Hubble parameter is given by

$$\mathcal{H} = \left(\frac{4\pi^3}{45} g_*\right)^{1/2} \frac{T^2}{M_P}\,, \tag{22}$$

where natural units $\hbar = c = 1$ have been employed, $T$ is temperature and $M_P$ is the Planck mass. The effective number of massless degrees of freedom $g_*$ is

$$g_* = \sum_{\text{bosons}} g_i \left(\frac{T_i}{T}\right)^4 + \frac{7}{8} \sum_{\text{fermions}} g_i \left(\frac{T_i}{T}\right)^4\,, \tag{23}$$

where $g_i$ counts the internal states of species $i$. Light neutrinos contribute to the sum over fermionic species. If particle of type $i$ is in thermal contact with the plasma, then $T_i = T$. If the expansion rate is smaller than the rate for a given process (e.g. a nuclear reaction), then that process will be dynamically important.

The second BBN role arises from electron neutrinos and antineutrinos transforming protons into neutrons and vice-versa through the reactions

$$\nu_e n \leftrightarrow e^- p, \qquad \overline{\nu}_e p \leftrightarrow e^+ n\,. \tag{24}$$

When chemical equilibrium obtains, the ratio of neutron to proton number densities is given by

$$\frac{n_n}{n_p} = \exp\left(-\frac{m_n - m_p}{T} - \frac{\mu_{\nu_e}}{T}\right)\,, \tag{25}$$

where $\mu_{\nu_e}$ is the electron neutrino chemical potential. A crucial event just prior to BBN is *weak freeze out*, when the reaction rates for equation (24) drop below $\mathcal{H}$. These reactions are then no longer rapid enough to maintain the $n/p$ ratio at its equilibrium value, and neutron decay becomes important. The $n/p$ ratio determines the amount of primordial $^4$He synthesized, because to a good first approximation all available neutrons are incorporated into this species. "Standard BBN" sees $\mu_{\nu_e}$ arbitrarily set to zero. However, there is no known fundamental reason to require $\mu_{\nu_e} = 0$. Neutrino oscillations can lead to time dependent neutrino chemical potentials, with a direct impact on BBN through the $n/p$ ratio.

The mean total collision rate $\langle \Gamma_\alpha \rangle$ for neutrino $\nu_\alpha$ ($\alpha = e, \mu, \tau$) in the epoch of the early universe after $\mu/\overline{\mu}$ disappearence is

$$\langle \Gamma_{\nu_\alpha} \rangle \simeq \kappa_\alpha G_F^2 T^5 \,, \tag{26}$$

where $\kappa_e \simeq 4$, $\kappa_{\mu,\tau} \simeq 2.9$ and $G_F$ is the Fermi constant. The average is taken over a Fermi-Dirac (FD) distribution

$$N^{eq}(p, \mu_{\nu_\alpha}, T) \equiv \frac{p^2}{2\pi^2} f^{eq}(\frac{p}{T}, \frac{\mu_{\nu_\alpha}}{T}) = \frac{1}{2\pi^2} \frac{p^2}{e^{\frac{p-\mu_{\nu_\alpha}}{T}} + 1} \,, \tag{27}$$

where $p \simeq E$ is the magnitude of the three-momentum of the neutrino. The chemical potential $\mu_{\nu_\alpha}$ has been arbitrarily equated to zero in computing the righthand side of equation (26). If antineutrinos are zero chemical potential FD distributed, then their mean collision rates are also given by equation (26). Note that the total equilibrium number density $n_{\nu_\alpha}$ is given by

$$n_{\nu_\alpha}(\mu_{\nu_\alpha}, T) = \int_0^\infty N^{eq}(p, \mu_{\nu_\alpha}, T)\, dp \,. \tag{28}$$

If we take the constituents of the plasma at this epoch to be free of exotic states such as light sterile neutrinos, light neutral spin-0 bosons and the like, then from

equations (22) and (23) the expansion rate of the universe is

$$\mathcal{H} \simeq 5.44 \frac{T^2}{M_P}\,, \tag{29}$$

with $g_* = 10.75$ under the stated assumptions.

Neutrino collisions will be very important for all temperatures above the decoupling temperature, $T_{\nu_\alpha}$, defined through

$$\kappa_\alpha G_F^2 T_{\nu_\alpha}^5 \simeq 5.44 \frac{T_{\nu_\alpha}^2}{M_P} \Rightarrow T_{\nu_\alpha} \simeq 1 \text{ MeV}\,. \tag{30}$$

Above about 1 MeV, collisions keep neutrinos in thermal equilibrium with the electrons, positrons, photons and the other neutrinos and antineutrinos. Also, neutrino oscillations will be collision affected in this regime, necessitating the use of the Quantum Kinetic Equation formalism (4, 5, 31–36). Since BBN begins at about 0.4 MeV, the neutrinos are expected to be propagating in a collisionless way during the BBN epoch itself. However, the initial conditions for BBN (such as the $n/p$ ratio at freeze-out) depend on the collision-affected neutrino dynamics of the previous epoch.

Naively, one would hope to focus on oscillation dynamics involving the three known neutrinos $\nu_{e,\mu,\tau}$. However, most of the interesting work has focussed on active-sterile neutrino oscillations. The reasons for this are, first, that sterile neutrinos can have dramatic consequences for BBN, and, second, the Quantum Kinetic Equations for an active-sterile system, equation (4), are much simpler than for its active-active counterpart, equation (5).

Active-active oscillations are often neglected in the literature because of the common assumption that all neutrino chemical potentials are zero, or at least extremely small. If the chemical potentials are in fact nonzero, then an important consequence is the inequality of neutrino and antineutrino number densities of a

given flavor. Define the *$\alpha$-flavor neutrino asymmetry* $L_{\nu_\alpha}$ by

$$L_{\nu_\alpha} \equiv \frac{n_{\nu_\alpha} - n_{\overline{\nu}_\alpha}}{n_\gamma} \,. \tag{31}$$

When thermal equilibrium holds this evaluates to

$$L_{\nu_\alpha} \simeq \frac{1}{24\zeta(3)} \left[ \pi^2 (\xi_{\nu_\alpha} - \overline{\xi}_{\nu_\alpha}) - 6(\xi^2_{\nu_\alpha} - \overline{\xi}^2_{\nu_\alpha}) \ln 2 + (\xi^3_{\nu_\alpha} - \overline{\xi}^3_{\nu_\alpha}) \right] , \tag{32}$$

where $\xi_{\nu_\alpha} \equiv \mu_{\nu_\alpha}/T$, $\overline{\xi}_{\nu_\alpha} \equiv \mu_{\overline{\nu}_\alpha}/T$ are dimensionless chemical potentials. This equation is exact if $\overline{\xi}_{\nu_\alpha} = -\xi_{\nu_\alpha}$, otherwise it is a good approximation for $|\xi| \lesssim 1$. It is convenient to scale the neutrino number density with the photon number density, and to consider the $\xi$'s in place of the $\mu$'s, because the scaled quantities do not red-shift. While processes such as $\nu_\alpha \overline{\nu}_\alpha \leftrightarrow e^+ e^- \leftrightarrow \gamma\gamma$ are occurring quickly relative to the expansion rate, the neutrinos and antineutrinos are in chemical equilibrium which requires $\xi_{\nu_\alpha} + \overline{\xi}_{\nu_\alpha} = \xi_{e^-} + \xi_{e+} = 0$, so equation (32) is then exact.

The assumption that $\nu/\overline{\nu}$ chemical potentials are zero, or perhaps of the tiny magnitude motivated by the baryon/electron asymmetries, is one of the defining features of standard BBN. However, the equal number densities so implied for all active neutrino species render neutrino oscillations cosmologically uninteresting, simply because equal distributions would just be exchanged through the oscillations. We will therefore concentrate on cases featuring unequal distribution functions. A few well motivated situations of this sort are:

1. *Sterile neutrinos.* They would decouple very early, with subsequent reheating processes greatly diluting the putative sterile component of the plasma, so that by the epoch immediately prior to BBN their number density would be effectively zero. Active-sterile oscillations could then repopulate the plasma with sterile neutrinos.

2. *Mirror neutrinos.* They are similar to sterile neutrinos, except that they have weak-scale self-interactions, and their small initial number densities are justified differently (37–40).

3. *Active neutrinos in the presence of large chemical potential differences between the flavors.* As we will see, active-sterile oscillations can create reasonably large chemical potentials during the epoch preceeding BBN (41). After this has happened, other oscillation modes, including active-active channels, can reprocess the flavor of the lepton asymmetry (42). In addition, large chemical potentials can be created during much earlier epochs, for example by an Affleck-Dine mechanism (43, 44), which can be similarly reprocessed.

## *4.2 Active-Sterile Oscillations: Formalism*

### 4.2.1 Quantum Kinetic Equations

Equations (5) and (6) describe the evolution of the 1-body reduced density matrix $\rho$ for an active-sterile system. The antineutrino system is described by a similar equation for $\overline{\rho}$.

The diagonal entries of $\rho$ ($\overline{\rho}$) are appropriately normalized distribution functions for $\nu_\alpha$ ($\overline{\nu}_\alpha$) and $\nu_s$ ($\overline{\nu}_s$):

$$N_{\nu_\alpha}(p,T) = \frac{1}{2}[P_0(y,T) + P_z(y,T)]\ N^{eq}(p,0,T)\,, \tag{33}$$

$$N_{\nu_s}(p,T) = \frac{1}{2}[P_0(y,T) - P_z(y,T)]\ N^{eq}(p,0,T)\,, \tag{34}$$

where $N^{eq}(p,0,T)$ is the often-used reference distribution function. The antineutrino distribution functions are given similarly. Since we have defined $P_{0,z}$ to be ratios of distribution functions, there is no term in the QKEs related to the

expansion of the universe. It is understood, however, that a neutrino which has momentum $p$ at temperature $T$ will red-shift to momentum $p'$ at temperature $T'$ such that $p/T = p'/T'$. In other words, the scaled momentum

$$y \equiv \frac{p}{T} \tag{35}$$

is the natural and most convenient variable. Note that $y$ has nothing to do with the unit vector $\hat{y}$.

The function $\mathbf{V}(y,T)$, describing the quantally coherent part of the evolution, is given by

$$\mathbf{V}(y,T) = \beta(y,T)\hat{x} + \lambda(y,T)\hat{z}\,, \tag{36}$$

with

$$\beta(y,T) = \frac{\Delta m^2}{2yT}\sin 2\theta_0, \quad \lambda(y,T) = -\frac{\Delta m^2}{2yT}\cos 2\theta_0 + V_\alpha(y,T)\,, \tag{37}$$

where $\Delta m^2$ and $\theta_0$ are, respectively, the mass-squared difference and vacuum mixing angle for $\nu_\alpha - \nu_s$ oscillations. The mass eigenstate neutrinos $\nu_{a,b}$ are defined by $\nu_\alpha = \cos\theta_0\nu_a + \sin\theta_0\nu_b$, $\nu_s = -\sin\theta_0\nu_a + \cos\theta_0\nu_b$, with $\theta_0$ defined so that $\cos 2\theta_0 \geq 0$ and $\Delta m^2 \equiv m_b^2 - m_a^2$. The function $V_\alpha$ is the effective matter potential (45, 46). Calculated to the appropriate order for our applications, it is given by (47)

$$V_\alpha(y,T) = \frac{\Delta m^2}{2yT}[-a(y,T) + b(y,T)]\,, \tag{38}$$

with the dimensionless functions $a(y,T)$ and $b(y,T)$ being

$$a(y,T) = -\frac{4\zeta(3)\sqrt{2}}{\pi^2}\frac{G_F T^4 y}{\Delta m^2}L^{(\alpha)}\,, \quad b(y,T) = -\frac{4\zeta(3)\sqrt{2}A_\alpha}{\pi^2}\frac{G_F T^6 y^2}{\Delta m^2 m_W^2}\,, \tag{39}$$

where $m_W$ is the $W$-boson mass, $A_e \simeq 17$, $A_{\mu,\tau} \simeq 4.9$ and the $\alpha$-type *effective neutrino asymmetry* is defined by

$$L^{(\alpha)} = L_{\nu_\alpha} + L_{\nu_e} + L_{\nu_\mu} + L_{\nu_\tau} + \eta. \tag{40}$$

Observe that $\mathbf{V}$ depends on $\rho$ through the dependence of $a$ on $L_{\nu_\alpha}$, making the asymmetry evolution non-linear. The quantity $\eta$ is a small term related to the cosmological baryon-antibaryon asymmetry. For antineutrinos, the corresponding function $\overline{\mathbf{V}}$ is obtained from $\mathbf{V}$ by replacing $L^{(\alpha)}$ by $-L^{(\alpha)}$.

The Mikheyev-Smirnov-Wolfenstein (MSW) resonance conditions are (45–47)

$$\cos 2\theta_0 + a(y,T) - b(y,T) = 0, \quad \cos 2\theta_0 - a(y,T) - b(y,T) = 0\,, \tag{41}$$

for neutrinos and antineutrinos, respectively. It is important to appreciate that the resonance conditions at a given temperature are met only for neutrinos (antineutrinos) of a certain momentum $y_{res}$ ($\overline{y}_{res}$).

The decoherence function is $D(y,T) = \Gamma_{\nu_\alpha}(y,T)/2$, with $\Gamma_{\nu_\alpha}(y,T)$ being the total collision rate for $\nu_\alpha$'s with momentum $y$. When thermal and chemical equilibria hold,

$$\Gamma_\alpha(y,T) = \kappa_\alpha \frac{180\zeta(3)}{7\pi^4} G_F^2 T^5 y + O(L)\,, \tag{42}$$

where the $O(L)$ term takes care of possible asymmetries in the medium. The antineutrino decoherence function is obtained by reversing the signs of all the asymmetries.

The function $D$ is in general a dynamical quantity because the collision rates depend on the neutrino distribution functions and hence on $\rho$. However, it approximates to the external function displayed above provided that thermal equilibrium obtains and all lepton numbers are small (but not necessarily tiny). This greatly simplifies the numerical solution of the equations. Fermi factors have been neglected in the calculation of $D$, and also the repopulation function $R$ discussed below.

The repopulation function $R$ is approximately given by

$$R(y,T) = \Gamma_\alpha(y,T)\left\{\frac{N^{eq}(p,\xi_\alpha,T)}{N^{eq}(p,0,T)} - \frac{1}{2}[P_0(y,T) + P_z(y,T)]\right\}, \qquad (43)$$

when all distribution functions except that for $\nu_\alpha$ are of FD form, and the $\nu_\alpha$ distribution is approximately FD. The physical interpretation of this expression is that all weak interaction processes involving $\nu_\alpha$ are tending to send its actual distribution function towards equilibrium FD form. For antineutrinos, $\overline{R}$ is obtained from $R$ by replacing $\xi_{\nu_\alpha}$ by $\overline{\xi}_{\nu_\alpha}$ and the $P$'s by $\overline{P}$'s.

### 4.2.2 The Adiabatic Limit

The Quantum Kinetic Equations in principle provide a complete solution to oscillating neutrino dynamics in this context. Indeed, numerical solutions to these equations have been computed for certain situations (40, 48–50). (Numerical work which considers the simplified case where the full energy spectrum of neutrinos is replaced by the mean momentum can be found, for instance, in Refs. (36, 41, 51–54). For calculations in a collisionless regime, see Refs. (55, 57, 58).) Before reviewing some of these results, it will be helpful to extract some analytical understanding of important features of the dynamics (41, 48, 56, 59, 60). It turns out that taking the adiabatic limit is a useful analytical strategy. The functions $\beta$, $\lambda$, $D$ and $R$ all depend on time or temperature. The adiabatic limit is useful when the rates of change of these quantities are sufficiently small (56).

Consider first the higher temperature regime where collisions maintain the $\nu_\alpha$'s (and $\overline{\nu}_\alpha$'s) close to thermal equilibrium, so that we can adopt the *instantaneous repopulation approximation*, whereby

$$\frac{P_0(y,T) + P_z(y,T)}{2} \simeq \frac{N^{eq}(p,\xi_\alpha,T)}{N^{eq}(p,0,T)} \qquad (44)$$

is maintained at all times, though possibly with a time-dependent chemical potential. It turns out that the further approximation $R \simeq 0$ is reasonable in this regime, although its use is not strictly necessary in developing the adiabatic limit (60). However, the extra algebra involved when $R \neq 0$ obscures rather than clarifies, so we will set $R = 0$ for pedagogical reasons. Note also that $R \simeq 0$ is a valid approximation for $T < 1$ MeV because weak collision effects are then unimportant ($D \simeq 0$ also holds in this case).

With $R \simeq 0$, the QKEs simplify to

$$\frac{\partial}{\partial t}\begin{pmatrix} P_x \\ P_y \\ P_z \end{pmatrix} \simeq \begin{pmatrix} -D & -\lambda & 0 \\ \lambda & -D & -\beta \\ 0 & \beta & 0 \end{pmatrix}\begin{pmatrix} P_x \\ P_y \\ P_z \end{pmatrix}, \tag{45}$$

or, in a self-evident matrix notation,

$$\frac{\partial \mathbf{P}}{\partial t} \simeq \mathcal{K}\mathbf{P}\,. \tag{46}$$

We have dropped the explicit $(y, T)$ dependence for notational simplicity.

To solve equation (46), we first introduce the *instantaneous diagonal basis* through

$$\mathbf{Q} = \mathcal{U}\mathbf{P}\,, \tag{47}$$

where $\mathcal{U}$ is a time-dependent matrix that diagonalizes $\mathcal{K}$,

$$\mathcal{K}_d \equiv \mathrm{diag}(k_1, k_2, k_3) = \mathcal{U}\mathcal{K}\mathcal{U}^{-1}\,, \tag{48}$$

with $k_{1,2,3}$ being eigenvalues. In the instantaneous diagonal basis, equation (46) becomes

$$\frac{\partial \mathbf{Q}}{\partial t} \simeq \mathcal{K}_d\mathbf{Q} - \mathcal{U}\frac{\partial \mathcal{U}}{\partial t}^{-1}\mathbf{Q}\,. \tag{49}$$

The *adiabatic limit* of equation (46) is defined by the approximation

$$\mathcal{U}\frac{\partial \mathcal{U}}{\partial t}^{-1} \simeq 0\,. \tag{50}$$

Equation (49) is then formally solved to yield

$$\mathcal{P}(t) = \mathcal{U}^{-1}(t) e^{\int_0^t \mathcal{K}_d(t')dt'} \mathcal{U}(0)\mathcal{P}(0)\,. \tag{51}$$

The time dependences of the various quantities have been reinstated for obvious reasons.

Under most circumstances, for instance $|\lambda| \gg D$ and $|\beta| \gg D$ individually, the eigenvalue spectrum consists of a complex conjugate pair (56, 59),

$$k_{1,2} \equiv -d \pm i\omega\,, \tag{52}$$

together with a negative (real) eigenvalue,

$$k_3 = -\frac{\beta^2 D}{d^2 + \omega^2}\,. \tag{53}$$

The easily derived relations,

$$d = D + \frac{k_3}{2}, \tag{54}$$

$$\omega^2 = \lambda^2 + \beta^2 + k_3 D + \frac{3}{4}k_3^2\,, \tag{55}$$

should also be noted. It is useful to call $d$ the *oscillation-affected decoherence function* and $\omega$ the *matter- and collision-affected oscillation frequency*. The very important third eigenvalue $k_3$ is the relaxation rate for the $\nu_\alpha \leftrightarrow \nu_s$ process (see below). For many applications $|k_3|$ is small, so that $d \simeq D$ and $\omega \simeq \sqrt{\lambda^2 + \beta^2}$. In order to use equation (51), the diagonalization matrices must also be computed. The explicit expressions can be found in Refs. (56, 59).

The adiabatic limit solution supplies a useful picture for the dynamics (in its domain of applicability (56) of course). (Some of the following insights were obtained earlier using a related approach (41, 48).) Consider first the case of zero decoherence, $D = 0$. This situation obtains after neutrino decoupling. The

eigenvalues $k_i$ are then (56, 59)

$$k_1 = k_2^* = i\sqrt{\beta^2 + \lambda^2}\,, \quad k_3 = 0\,, \tag{56}$$

where $\omega = \sqrt{\beta^2 + \lambda^2}$ is in this case exactly equal to the usual matter-affected oscillation frequency. The adiabatic solution of equation (51) is then just a restatement of the usual adiabatic matter-affected evolution one obtains by solving the Schrödinger Equation. For instance, one can show that equation (51) becomes

$$P_z(t) = \cos 2\theta_m(t) \cos 2\theta_m(0)\,, \tag{57}$$

with the initial conditions $P_{x,y}(0) = 0$ and $P_{z,0}(0) = 1$ (i.e. no sterile neutrinos initially). The function $\cos 2\theta_m \equiv \lambda/\sqrt{\lambda^2 + \beta^2}$ is the cosine of twice the standard matter-affected mixing angle. The oscillatory terms arising from $k_{1,2}$ have been taken to average to zero. This is the standard adiabatic MSW result. For instance if the effective matter potential (and hence $\lambda$) varies from $+\infty$ at $t = 0$ to $-\infty$ at $t = \infty$ through the resonance $\lambda = 0$, then $P_z$ evolves from 1 to $-1$, signalling complete $\nu_\alpha \to \nu_s$ conversion. A simple physical picture then results: as neutrinos with momentum $y$ cross a narrow MSW resonance centered at $y = y_{res}$, adiabaticity guarantees full $\nu_\alpha \leftrightarrow \nu_s$ conversion. (Similarly antineutrinos, but note that $\overline{y}_{res} \neq y_{res}$ when $L^{(\alpha)} \neq 0$.) For a narrow resonance, the QKEs can be approximated by equations which relate the rates of change of the distribution functions to the speeds at which the resonance momenta move through the distributions (42, 61). In practice, such an approximation can often also be validly used for temperatures slightly higher than 1 MeV.

Now consider the opposite case, where collisional effects dominate. The real parts of $k_{1,2}$ then completely damp the oscillatory behaviour driven by the imaginary parts, and a nonzero $k_3$ enters the game. Equation (51) then allows one to

solve for the coherence function $P_y$ in terms of $P_z$, yielding

$$P_y(t) \simeq \frac{k_3(t)}{\beta(t)} P_z(t)\,. \tag{58}$$

(One can also solve for $P_x$.) Substituting for $P_y$ in equation (45), one obtains

$$\frac{\partial P_z}{\partial t} \simeq k_3 P_z \tag{59}$$

as a self-contained differential equation for $P_z$ and hence for the distribution functions. (A similar equation follows for antineutrinos.) Because the coherences $P_{x,y}$ have been eliminated, one can speak of the *classical Boltzmann limit* of the QKEs. Because $k_3$ is negative, and under most interesting circumstances much smaller in magnitude than the decoherence rate $D$, equation (59) describes a relatively slow collision-dominated evolution of $P_z$ towards zero, that is, towards $N_{\nu_\alpha} = N_{\nu_s}$. It can be viewed as a relaxation effect.

### 4.2.3 Neutrino Asymmetry Evolution

Neutrino asymmetries and chemical potentials are important quantities. As previously explained, active-active oscillations are expected to have strong effects only if $e$, $\mu$ and $\tau$ asymmetries are unequal, and an $e$-like asymmetry directly affects BBN through the proton-neutron interconversion reactions. Furthermore, the effective matter potential of equation (38) has a term proportional to a linear combination of asymmetries. Large asymmetries therefore imply small matter-affected mixing angles $\theta_m$, and hence suppressed oscillations. This is of particular concern for sterile neutrino models: sufficiently large asymmetries will suppress active to sterile oscillations with important implications for the consistency of these models with BBN.

Using the QKEs together with $\alpha+s$ lepton number conservation, one can easily

show that

$$\frac{dL_{\nu_\alpha}}{dt} = \frac{1}{2n_\gamma}\int \beta(P_y - \overline{P}_y)N^{eq}(p,0,T)dp \tag{60}$$

is the evolution equation for $L_{\nu_\alpha}$ under the action of $\nu_\alpha \leftrightarrow \nu_s$ and $\overline{\nu}_\alpha \leftrightarrow \overline{\nu}_s$ oscillations. We will study this simple two-flavor toy model before considering more realistic scenarios.

The QKEs can be numerically integrated to yield asymmetry evolution curves. (For numerical reasons, it is useful to include equation (60) in the coupled system, even though it is redundant). Let us suppose that all neutrino asymmetries start out being small, perhaps of the order of the observed baryon asymmetry $\sim 10^{-10}$. There is no guarantee that this is realistic, but up to now most of the interesting work in the literature has focussed on this case. When $\Delta m^2 < 0$ and the vacuum mixing angle is small, there is a large range of parameters for which explosive asymmetry growth begins at a certain critical temperature $T_c$, as displayed in Figure 7. This is a runaway positive feedback phenomenon that occurs when an $L^{(\alpha)} = 0$ approximate fixed point changes from being stable to unstable at $T = T_c$ (41,48). After a short spurt of quasi-exponential growth, the evolution settles into a less dramatic but still significant approximate power law phase, before reaching a steady state plateau at a value in the range $0.2 - 0.35$ (depending on the oscillation parameter choice) (42).[6] The baryon asymmetry in the plasma, which couples in through the $\eta$-term in $L^{(\alpha)}$, seeds the neutrino asymmetry growth. The existence of the asymmetry growth effect must be carefully taken into account when calculating sterile neutrino production for BBN purposes.

The main features of the asymmetry growth curves have been understood, and

[6]Reference (62) found much smaller values for the final asymmetries. A critique of this work can be found in Ref. (63). See also Refs. (64, 65).

are discussed in some detail in Refs. (41, 42, 48, 63). In a nutshell, the explosive growth phase is governed by the collision dominated dynamics leading to equations (58) and (59), while the approximate power law regime has adiabatic MSW transitions as the driving force. It has been shown that asymmetry growth resembling that shown in Figure 7 will occur for the parameter space region

$$\Delta m^2 < 0 \quad \text{with} \quad |\Delta m^2| \gtrsim 10^{-4}\ \text{eV}^2\,,$$
$$10^{-10} \lesssim \sin^2 2\theta_0 \lesssim \text{few} \times 10^{-5} \left(\tfrac{\text{eV}^2}{|\Delta m^2|}\right)^{1/2}\,. \tag{61}$$

For $|\Delta m^2| < 10^{-4}$ eV$^2$, asymmetry can be generated, but it tends to be oscillatory (36, 51, 55, 57). Values of $\sin^2 2\theta_0$ smaller than $10^{-10}$ are too small to generate an asymmetry, while values exceeding the upper bound above lead to copious sterile neutrino production which is also detrimental to asymmetry growth. One can also show that the critical temperature $T_c$ is roughly given by

$$T_c \sim (16 \to 20\ \text{MeV}) \left(\frac{|\Delta m^2| \cos 2\theta_0}{\text{eV}^2}\right)^{1/6}\,. \tag{62}$$

### *4.3 Active-Sterile Oscillations: Applications*

#### 4.3.1 Sterile Neutrino Production

For the moment, let us continue to study the toy universe where only $\nu_\alpha \leftrightarrow \nu_s$ and $\overline{\nu}_\alpha \leftrightarrow \overline{\nu}_s$ oscillations occur (for a particular $\alpha$). An interesting question is: for a given choice of $\Delta m^2$ and $\theta_0$, how does sterile neutrino production affect BBN? For $\alpha = \mu$ or $\tau$ the effect is restricted to potentially increasing the energy density in relativistic species and hence the expansion rate of the universe. (Note that for $\Delta m^2 \lesssim 10^{-7}$ eV$^2$ significant $\nu_{\mu,\tau} \leftrightarrow \nu_s$ oscillations can occur only after neutrino decoupling, so the overall energy density is unaffected.) For $\alpha = e$, the possible effects are more complicated. Because of the reactions in equation

(24), the possible existence of an $e$-like asymmetry must be carefully considered, and one has to take into account the effect of distortion and depletion of the $\nu_e$ spectrum below the decoupling temperature (36, 55, 57).

The detailed results will clearly depend on whether or not the plasma has large neutrino asymmetries. As we have just seen, an $\alpha$-like asymmetry will be generated during the $T \sim 10$'s of MeV epoch by oscillations if the parameters obey equation (61). Other mechanisms, such as Affleck-Dine, can create large asymmetries at much higher temperatures. Unfortunately, prospects for directly detecting the relic neutrino sea remain remote, so there is much room for theoretical speculation.

The important pioneering works on sterile neutrino production were performed before the asymmetry generation effect was understood (66–71). By neglecting the baryon asymmetry and setting all neutrino asymmetries to zero, one obtains a simplified system driven by identical neutrino and antineutrino oscillation dynamics which are decoupled from each other. For $\Delta m^2 > 0$, this simplification is consistent. However, for $\Delta m^2 < 0$, the $L^{(\alpha)} = 0$ approximate fixed point becomes unstable and the zero asymmetry constraint is not justified.

A useful summary of the pioneering results is contained in Figures 2 and 4 from Ref. (69). These plots show contours in the $\Delta m^2 - \sin^2 2\theta_0$ plane corresponding to different values of $g_{max}$, a parameter which quantifies sterile neutrino contribution to the expansion rate, equation (22), through an effective increase in the number of fermionic degrees of freedom contributing to $g_*$. (We will call this parameter $\Delta N_{eff}$ from now on. Note that for $\alpha = e$ its meaning is more subtle (69).) The precise constraint one should use is at this stage unclear, because of uncertainties in the primordial light element abundance observations. Nevertheless, these plots

provide interesting information for neutrino model builders. For instance, a $\nu_\mu \to \nu_s$ solution to the atmospheric neutrino problem with $\Delta m^2 \sim 10^{-2.5}$ eV$^2$ and $\sin^2 2\theta_0 \sim 1$ would appear to go hand-in-hand with a fully thermalized $\nu_s$ prior to BBN. Such a situation would be cosmologically disfavored because of concomitant $^4$He overproduction.

As already noted, for $\Delta m^2 < 0$ one has to take into account the asymmetry generation that occurs simultaneously with sterile neutrino production. The qualitative effect is clear: because asymmetries suppress oscillations, the rigorous $\Delta m^2 < 0$ bounds should be weaker than those displayed in Figure 4 of Ref. (69), for example. However, detailed calculations (48, 72) reveal that the asymmetry amplification process does not modify the "traditional" bounds by very much, except when the BBN constraint on $\Delta N_{eff}$ is taken to be rather stringent, say $\Delta N_{eff} < 0.1$. The reason for this is that sterile neutrino production tends to delay the onset of asymmetry growth (see Figure 12 of Ref. (72) for a clear illustration).

All of the above related to the artificial two-flavor $\nu_\alpha/\nu_s$ case. But the most dramatic consequence of asymmetry creation occurs in more realistic multiflavor situations. This is simply because an asymmetry created by one active-sterile oscillation mode can suppress a *different* active-sterile mode (41, 48, 49, 72). The most studied case was motivated by the atmospheric neutrino problem. As noted above, the $\nu_\mu \to \nu_s$ solution to the atmospheric neutrino problem appears at first sight to be cosmologically disfavored. However, tiny mixing between the $\nu_s$ and a more massive $\nu_\tau$ can completely change the dynamics, because the nonzero $L_{\nu_\tau}$ created by the small-angle, negative $\Delta m^2$ $\nu_\tau \to \nu_s$ mode can suppress the $\nu_\mu \to \nu_s$ oscillations that would be very strong otherwise. Explicit calculations show that

if the mass eigenvalues associated with the $\nu_\mu/\nu_s$ subsystem are much less than an eV, then a $\nu_\tau$ mass at the few eV level or higher is required (41, 48, 49, 72). (Though somewhat large values were obtained in Ref. (73), the later independent results of Ref. (72) agree with the original results of Refs. (41, 48).)

#### 4.3.2 $e$-Like Asymmetry and $^4$He Abundance.

Suppose a small-angle active-sterile mode with a relatively large but negative $\Delta m^2$ creates a large asymmetry of a certain flavor fairly early. Later on, it is certainly possible for other oscillation modes to reprocess the flavor of the asymmetry. For instance, small-angle $\nu_\tau \to \nu_s$ oscillations might create a large $L_{\nu_\tau} \sim 0.3$ which gets reprocessed into a reasonably large (say $\sim 0.01$) $L_{\nu_e}$ by $\nu_\tau \leftrightarrow \nu_e$ oscillations. Recall that the usually innocuous active-active modes can become important after flavor asymmetries get created.

Several scenarios of this type have been investigated in the literature (40,42,61, 74). One has to study the peculiarities of each neutrino model on a case-by-case basis. The more flavors one has, the more complicated the analysis becomes. The most ambitious attempt to date relates to the mirror matter model with three active and three mirror neutrino flavors (40).

By way of example, Ref. (42) considered a model with the three active neutrinos and one light sterile flavor with the mass hierarchy $m_{\nu_\tau} \gg m_{\nu_\mu}, m_{\nu_e}, m_{\nu_s}$. A $\tau$-flavor asymmetry is first created by the $\nu_\tau \leftrightarrow \nu_s$ mode, and subsequently reprocessed into $e$- and $\mu$-like asymmetries by $\nu_\tau \leftrightarrow \nu_e$ and $\nu_\tau \leftrightarrow \nu_\mu$ oscillations. The $e$-like asymmetry is of most interest because of its role in the neutron-proton interconversion reactions. Final values for $L_{\nu_e}$ around $0.02(T_{\nu_e}/T_\gamma)^3$ for $\Delta M^2 > 10$ eV$^2$ were found, where $\Delta M^2$ is the squared-mass splitting between

$\nu_\tau$ and the lighter flavors. The effect of such an asymmetry on $^4$He abundance is roughly equivalent to *reducing* the expansion rate by, effectively, half of a neutrino: $\Delta N_{eff} \sim -0.5$. Note that the sign of the asymmetry is crucial here: positive $L_{\nu_e}$'s reduce the $^4$He yield (equivalent to reducing the expansion rate), while negative values increase the yield (equivalent to increasing the expansion rate). The sign of $L_{\nu_e}$ is controlled by the sign of the $L_{\nu_\tau}$ originally created, which in turn is controlled by the unknown initial (high $T$) values of the asymmetries. It turns out that the results quoted above assume initial conditions that lead to a positive $L_{\nu_\tau}$.

Clearly, the relevance or otherwise of these studies for understanding nature hinges on the as yet unclear existential status of light sterile neutrinos. Future terrestrial experiments such as SNO, MiniBOONE and the long baseline projects will help to clarify the situation. Better information about the mass and mixing angle spectrum for neutrinos will be needed, as well as better information about primordial light element abundances. Precision cosmic microwave background measurements also have a role to play by helping to pin down the baryon density (a crucial input into BBN calculations), as well as the expansion rate of the universe at the time of photon decoupling (75–77).

### *4.4 Remarks About Active-Active Oscillations*

Collision-affected active-active oscillations have received very little attention because the relevant Quantum Kinetic Equations are rather complicated, as can be seen by comparing equation (4) with equation (5). The studies that have been done typically focussed on collision-unaffected adiabatic transitions, for which a simpler treatment is possible. The works alluded to in the previous subsubsec-

tion in fact used such an approach. The collision-affected case remains largely virgin territory: the required QKEs have been written down (4, 5), but remain unsolved, except for a certain interesting special case (9, 78). The special situation is that of propagation through a "flavor-blind" medium. Examples include an active-active oscillating system traversing a dense nucleonic medium, and a $\nu_\mu/\nu_\tau$ system propagating through an electron-positron plasma. In both cases, the microscopic collisions do not distinguish between the flavors of the oscillating system. While the practical relevance of these systems is not entirely clear, a very interesting phenomenon has been discovered: synchronization of modes in the rapid collision limit. In vacuum, and in a refractive medium, neutrino oscillation lengths generally depend on energy. It has been found that rapid flavor-blind collisions force all modes to have the same oscillation length, which has been analytically proven to be a kind of thermal average of the oscillation lengths the neutrinos would have in the absence of the collisions. This leads at a sharpening of MSW transitions, and it reflects an interesting persistence-of-quantal-coherence effect which may find application outside of the neutrino domain (9).

## 5 NEUTRINOS IN SUPERNOVAE AND PROTO-NEUTRON STARS

The current gravitational core collapse supernova paradigm is based on the original suggestion by Colgate and White (79) that the explosion derives from neutrino energy deposition. However, since that time, much has been learned about neutrino–matter interactions that have modified the original model. It has also been realized that the implementation of accurate neutrino transport is critical, since the deposited energy is a small fraction ($\leq 1\%$) of the available gravitational

binding energy of the remnant ($\sim 3GM^2/5R \approx 3 \cdot 10^{53}(M/1.4\ \mathrm{M}_\odot)^2$ ergs).

The initial phases of the supernova begin with the destabilization and collapse of the core of a massive star (see Ref. (80) for the important physics which occurs during this period). The collapsing core, which is initially composed of iron peak elements with a net electron content $Y_e = n_e/n_B \simeq 0.41 - 0.43$, divides into two portions: an inner, homologous (with infall velocity roughly proportional to the radius) core and an outer region that collapses supersonically. The infalling matter maintains a nearly constant entropy per baryon $s \approx 1$; the entropy gain from out-of-equilibrium weak interactions is balanced by the energy loss from escaping neutrinos. During the collapse, electrons and protons are converted into neutrons and neutrinos as the matter attempts to maintain beta equilibrium. When the central density reaches about $10^{12}$ g cm$^{-3}$, neutrinos are unable to escape on dynamical timescales and are essentially frozen, or 'trapped', in the matter. The lepton number thereafter remains fixed, at a value of $Y_L = Y_e + Y_{\nu_e} \simeq 0.4$.

The collapse continues until the central density exceeds $n_0$ when the increased pressure from strong interactions reverses it. A shock is formed at the outer edge of the inner core (where sound waves from the center accumulate) and begins to propagate through the infalling outer region of the core. But this shock, called the "bounce" shock, stalls at a distance from the center of about 150 km, due to the energy expended in nuclear dissociation and neutrino losses. The stalled shock becomes an accretion shock which separates supersonically infalling matter from hot matter slowly settling onto the inner core, a PNS. After 10–20 ms, the overall structure evolves quasi-hydrostatically. The nucleons produced by the dissociation of heavy nuclei are heated by neutrino absorption from the

hot, newly formed PNS. Because neutrino emission varies as $T^6$, there is a point, known as the "gain radius", at which the heating exceeds the cooling.

Current calculations differ to some extent as to the outcome of this scenario, due to varying input physics and level of approximation to the neutrino transport problem. In addition, the negative entropy gradient that naturally exists is unstable against convection. This convection, which is neutrino-driven, seems to eventually assist in reviving the shock in some models. However, convection can only be realistically modeled in three dimensions, a task that is only beginning to be addressed. Additional fluid instabilities may also arise near the neutrinosphere, at which the neutrino optical depth to infinity is of order unity and where the neutrinos can begin to freely escape the star. The shock position during this hydrostatic epoch is determined by a delicate balance between thermal pressure caused by neutrino heating and the ram pressure of infalling matter (81). A successful supernova results if this balance becomes unstable, which could occur if the accretion shock can be maintained at a sufficient distance for a long enough time. The ram pressure decreases as material from less dense regions of the outer core is encountered, and could be eventually overcome by the more steady neutrino radiation from the core. Nevertheless, explosions in model simulations, even when they occur, appear to be marginal at best. Aside from uncertainties stemming from simulating 3-D, general relativisitic, neutrino transport, the initial structure of the pre-collapse core, the equation of state, and neutrino opacities and emissivities, all play roles in the outcome (82).

### 5.1 Role of Neutrinos in Gravitational Collapse Supernovae

Neutrino transport in the supernova environment is described by a Boltzmann tranport equation, derivable from the kinetic equation (4) by retaining only the diagonal elements in the density matrix $\rho(\mathbf{r}, \mathbf{r}')$. Even with this simplification, it is a nonlinear integro-partial differential equation that describes the time rate of change of the neutrino distribution function $f$. Advances made to date in the numerical solution of this equation in the supernova context may be found in Refs. (83). Historically, multigroup methods (in which the equation is discretized in energy groups) have involved moment expansions. When the temporal derivative of the first moment of $f$ is set to zero, a diffusion equation is obtained, but this cannot adequately handle the free-streaming regime at low densities. Flux limiting schemes have been used to bridge the diffusive and free-streaming regimes, but these are somewhat arbitrary and accurate calibration depends upon neutrino opacities and dynamics. In addition, there is a problem with the coupling of different neutrino-energy groups, especially because of $\nu - e$ scatterings, which involve large energy transfers. An additional complication in supernovae is that the approach to thermal and chemical equilibrium, and the conversion of diffusive flow to free streaming, occur simultaneously in space and time. Even with modern parallel supercomputers, it is necessary to integrate the Boltzmann equation over solid angles to reduce the dimensionality of the problem, with a corresponding loss of information about the neutrino angular distribution function. This could be important in regimes in which neutrino-driven convection, a 3-D phenomenon, is occuring.

Crucial weak interaction processes in the supernova environment include

$$p + e^- \rightarrow n + \nu_e, \quad (A, Z) + e^- \rightarrow (A, Z-1) + \nu_e \,, \tag{63}$$

$$\nu + (A, Z) \rightarrow \nu + (A, Z)\,, \tag{64}$$

$$\nu + e^- \rightarrow \nu + e^-, \qquad \nu + (A, Z) \rightarrow \nu + (A, Z)^*\,, \tag{65}$$

$$e^+ + e^- \rightarrow \nu + \bar{\nu}, \quad (A, Z)^* \rightarrow (A, Z) + \nu + \bar{\nu}, \quad (n, p) \rightarrow (n, p) + \nu + \bar{\nu}\,. \tag{66}$$

Reactions (63) begin the process of neutronization and decrease of $Y_L$, whose value after trapping determines the masses of the homologous core and initial PNS, and thus the available energy for the shock and subsequent neutrino emissions. The equation of state also influences these quantities, most importantly through the nuclear symmetry energy.

In the subnuclear density regime, the coherent scattering reaction (64) from nuclei in a lattice is the most important opacity source (see Section 3.2). The reactions (65) are important in changing the neutrino energy, and in achieving thermodynamic equilibrium. As referred to in Section 5.1, the large energy transfers of these processes is a hurdle for numerical calculations. The reactions (66) are also important in achieving thermodynamic equilibrium. The bremsstrahlung ($n+n \rightarrow n+n+\nu+\bar{\nu}$) and modified Urca ($n+p \rightarrow n+n+e^+ +\nu+\bar{\nu}$) processes involving nucleons dominate in many circumstances. For example, the production and thermalization of $\mu$ and $\tau$ neutrinos, which receives contributions from all the reactions (66), is dominated by nucleon bremsstrahlung for $n > 0.005$ and $T < 15$ MeV (84). The modified Urca process dominates the cooling of PNSs if direct Urca processes involving nucleons, hyperons or other strange particles do not occur.

### *5.2 Neutrinos From Proto-Neutron Stars*

A PNS is born in the aftermath of the gravitational collapse of the core of a massive star accompanying a successful supernova explosion. During the first

tens of seconds of evolution, nearly all ($\sim 99\%$) of the remnant's binding energy is radiated away in neutrinos of all flavors (85–90). The neutrino luminosities and the emission timescale are controlled by several factors, such as the total mass of the PNS and the opacity at supranuclear density, which depends on the composition and EOS. One of the chief objectives in modeling PNSs is to infer their internal compositions from neutrino signals detected from future supernovae like SuperK, SNO and others under consideration, including UNO (91).

### 5.2.1 General Description of the Birth of Proto-Neutron Stars

The evolution of a PNS proceeds through several distinct stages (2,85) and with various outcomes (25), as shown schematically in Figure 8. Immediately following core bounce and the passage of a shock through the outer PNS's mantle, the star contains an unshocked, low entropy core of mass $\simeq 0.7$ $M_\odot$ in which neutrinos are trapped (stage 1 in the figure). The core is surrounded by a low density, high entropy ($5 < s < 10$) mantle that is both accreting matter from the outer iron core falling through the shock and also rapidly losing energy due to electron captures and thermal neutrino emission. The mantle extends up to the shock, which is temporarily stalled about 200 km from the center prior to an eventual explosion.

After a few seconds (stage 2), accretion becomes less important if the supernova is successful and the shock has ejected the stellar envelope. Extensive neutrino losses and deleptonization will have led to a loss of lepton pressure and the collapse of the mantle. If enough accretion has occurred, however, the star's mass could increase beyond the maximum mass capable of being supported by the hot, lepton-rich matter. If this occurs, the remnant collapses to form a black hole and

its neutrino emission is believed to quickly cease (92).

Neutrino diffusion deleptonizes the core on time scales of 10–15 s (stage 3). Diffusion time scales are proportional to $R^2(c\lambda_\nu)^{-1}$, where $R$ is the star's radius and $\lambda_\nu$ is the effective neutrino mean free path. This generic relation illustrates how both the EOS and the composition influence evolutionary time scales. The diffusion of high-energy (200–300 MeV) $\nu$s from the core to the surface where they escape as low-energy (10–20 MeV) $\nu$s generates heat (a process akin to joule heating). The core's entropy approximately doubles, producing temperatures in the range of 30–60 MeV during this time, even as neutrinos continue to be prodiguously emitted from the star's effective surface, or $\nu-$sphere.

Strange matter, in the form of hyperons, a Bose condensate, or quark matter, suppressed when neutrinos are trapped, could appear at the end of the deleptonization. Its appearance would lead to a decrease in the maximum mass that matter is capable of supporting, implying metastability of the neutron star and another chance for black hole formation (25). This would occur if the PNS's mass, which must be less than the maximum mass of hot, lepton-rich matter (or else a black hole would already have formed), is greater than the maximum mass of hot, lepton-poor matter. However, if strangeness does not appear, the maximum mass instead increases during deleptonization and the appearance of a black hole would be unlikely unless accretion in this stage remains significant.

The PNS is now lepton-poor, but it is still hot. While the star has zero net neutrino number, thermally produced neutrino pairs of all flavors dominate the emission. The average neutrino energy slowly decreases, and the neutrino mean free path increases. After approximately 50 seconds (stage 4), $\lambda \simeq R$, and the star finally becomes transparent to neutrinos. Since the threshold density for the

appearance of strange matter decreases with decreasing temperature, a delayed collapse to a black hole is still possible during this epoch.

Following the onset of neutrino transparency, the core continues to cool by neutrino emission, but the star's crust remains warm and cools less quickly. The crust is an insulating blanket which prevents the star from coming to complete thermal equilibrium and keeps the surface relatively warm ($T \approx 3 \times 10^6$ K) for up to 100 years (stage 5). The temperature of the surface after the interior of the star becomes isothermal (stage 6) is determined by the rate of neutrino emission in the star's core and the composition of the surface.

### 5.2.2 The Proto-Neutron Star Evolution Equations

The equations that govern the transport of energy and lepton number in a PNS are obtained from the Boltzmann equation for massless particles (85, 88, 93, 94). We will focus on the non-magnetic, spherically symmetric situation, and note that fluid velocities are small enough so that hydrostatic equilibrium is nearly fulfilled. Under these conditions, the neutrino transport equations in a stationary metric

$$ds^2 = -e^{2\phi}dt^2 + e^{2\Lambda}dr^2 + r^2 d\theta^2 + r^2 \sin^2\theta \, d\Phi^2 \tag{67}$$

are:

$$\frac{\partial(N_\nu/n_B)}{\partial t} + \frac{\partial(e^\phi 4\pi r^2 F_\nu)}{\partial a} = e^\phi \frac{S_N}{n_B} \tag{68}$$

$$\frac{\partial(J_\nu/n_B)}{\partial t} + P_\nu \frac{\partial(1/n_B)}{\partial t} + e^{-\phi}\frac{\partial(e^{2\phi}4\pi r^2 H_\nu)}{\partial a} = e^\phi \frac{S_E}{n_B}\,, \tag{69}$$

where $n_B$ is the baryon number density and $a$ is the enclosed baryon number inside a sphere of radius $r$. The quantities $N_\nu$, $F_\nu$, and $S_N$ are the number density, number flux and number source term, respectively, while $J_\nu$, $H_\nu$, $P_\nu$, and $S_E$ are the neutrino energy density, energy flux, pressure, and the energy

source term, respectively.

In the absence of accretion, the enclosed baryon number $a$ is a convenient Lagrangian variable. The equations to be solved split naturally into a transport part, which has a strong time dependence, and a structure part, in which evolution is much slower. Explicitly, the structure equations are

$$\frac{\partial r}{\partial a} = \frac{1}{4\pi r^2 n_B e^{\Lambda}} \quad , \qquad \frac{\partial m}{\partial a} = \frac{\rho}{n_B e^{\Lambda}} \tag{70}$$

$$\frac{\partial \phi}{\partial a} = \frac{e^{\Lambda}}{4\pi r^4 n_B}\Big(m + 4\pi r^3 P\Big) \quad , \qquad \frac{\partial P}{\partial a} = -(\rho + P)\frac{e^{\Lambda}}{4\pi r^4 n_B}\Big(m + 4\pi r^3 P\Big) \tag{71}$$

The quantities $m$ (enclosed gravitational mass), $\rho$ (mass-energy density), and $P$ (pressure) include contributions from the leptons. To obtain the equations employed in the transport, equation (68) may be combined with the corresponding equation for the electron fraction

$$\frac{\partial Y_e}{\partial t} = -e^{\phi}\frac{S_N}{n_B} \tag{72}$$

to obtain

$$\frac{\partial Y_L}{\partial t} + e^{-\phi}\frac{\partial (e^{\phi} 4\pi r^2 F_{\nu})}{\partial a} = 0\,. \tag{73}$$

Similarly, equation (69) may be combined with the matter energy equation

$$\frac{dU}{dt} + P\frac{d(1/n_B)}{dt} = -e^{\phi}\frac{S_E}{n_B}\,, \tag{74}$$

where $U$ is the specific internal energy. The first law of thermodynamics yields

$$e^{\phi} T\frac{\partial s}{\partial t} + e^{\phi}\mu_{\nu}\frac{\partial Y_L}{\partial t} + e^{-\phi}\frac{\partial e^{2\phi} 4\pi r^2 H_{\nu}}{\partial a} = 0\,. \tag{75}$$

At high density and for $T \gg 1$ MeV, the source terms in the Boltzmann equation are sufficiently strong to ensure that neutrinos are in thermal and chemical equilibrium with matter. Thus, the neutrino distribution function in these regions is both nearly Fermi-Dirac and isotropic. We can approximate the distribution

function as an expansion in terms of Legendre polynomials to $O(\mu)$, which is known as the diffusion approximation. Explicitly,

$$f(\omega,\mu) = f_0(\omega) + \mu f_1(\omega)\,, \quad f_0 = [1 + e^{\left(\frac{\omega-\mu_\nu}{kT}\right)}]^{-1}\,, \tag{76}$$

where $f_0$ is the Fermi–Dirac distribution function at equilibrium ($T = T_{mat}$, $\mu_\nu = \mu_\nu^{eq}$), with $\omega$ and $\mu_\nu$ being the neutrino energy and chemical potential, respectively. In the diffusion approximation, $f_1(f_0)$ becomes (88)

$$f_1 = -D(\omega)\left[e^{-\Lambda}\frac{\partial f_0}{\partial r} - \omega e^{-\Lambda}\frac{\partial \phi}{\partial r}\frac{\partial f_0}{\partial \omega}\right]\,. \tag{77}$$

The explicit form of the diffusion coefficient $D$ is given by

$$D(\omega) = \left(j + \frac{1}{\lambda_a} + \kappa_1^s\right)^{-1}\,. \tag{78}$$

The quantity $j = j_a + j_s$, where $j_a$ is the emissivity and $j_s$ is the scattering contribution to the source term. The absorptivity is denoted by $\lambda_a$ and $\kappa_1^s$ is the scattering contribution to the transport opacity. Substituting

$$\frac{\partial f_0}{\partial r} = -\left(T\frac{\partial \eta_\nu}{\partial r} + \frac{\omega}{T}\frac{\partial T}{\partial r}\right)\frac{\partial f_0}{\partial \omega}\,, \tag{79}$$

where $\eta = \mu_\nu/T$ is the neutrino degeneracy parameter, in equation (77), yields

$$f_1 = -D(\omega)e^{-\Lambda}\left[T\frac{\partial \eta}{\partial r} + \frac{\omega}{Te^\phi}\frac{\partial (Te^\phi)}{\partial r}\right]\left(-\frac{\partial f_0}{\partial \omega}\right)\,. \tag{80}$$

Thus, the energy-integrated lepton and energy fluxes are

$$\begin{aligned} F_\nu &= -\frac{e^{-\Lambda}e^{-\phi}T^2}{6\pi^2}\left[D_3\frac{\partial (Te^\phi)}{\partial r} + (Te^\phi)D_2\frac{\partial \eta}{\partial r}\right] \\ H_\nu &= -\frac{e^{-\Lambda}e^{-\phi}T^3}{6\pi^2}\left[D_4\frac{\partial (Te^\phi)}{\partial r} + (Te^\phi)D_3\frac{\partial \eta}{\partial r}\right]\,. \end{aligned} \tag{81}$$

The coefficients $D_2$, $D_3$, and $D_4$ are defined by

$$D_n = \int_0^\infty dx\; x^n D(\omega) f_0(\omega)(1 - f_0(\omega))\,, \tag{82}$$

where $x = \omega/T$. These diffusion coefficients depend only on the microphysics of the neutrino-matter interactions. The fluxes appearing in the above equations are for one particle species. To include all six neutrino types, we redefine the diffusion coefficients in equation (81):

$$D_2 = D_2^{\nu_e} + D_2^{\bar{\nu}_e}\,, \quad D_3 = D_3^{\nu_e} - D_3^{\bar{\nu}_e}\,, \quad D_4 = D_4^{\nu_e} + D_4^{\bar{\nu}_e} + 4D_4^{\nu_\mu}\,. \tag{83}$$

### 5.2.3 Neutrino Luminosity from Proto-Neutron Stars

A fair representation of the signal in a terrestrial detector can be found from the time dependence of the total neutrino luminosity and average neutrino energy together with an assumption of a Fermi-Dirac spectrum with zero chemical potential. The total neutrino luminosity is globally the time rate of change of the star's gravitational mass, and due to energy conservation, is also

$$L_\nu = e^{2\phi} 4\pi r^2 H_\nu \tag{84}$$

at the edge of the star. However, since the spectrum is not precisely Fermi-Dirac at the neutrinosphere, a diffusion scheme only approximates the average energy. The average energy can be approximated as $< E_\nu > \approx 3T_\nu$, where $T_\nu$ is a mass-averaged temperature in the outermost zone.

Neutrino signals from PNSs depends on many stellar properties, including the mass; initial entropy, lepton fraction and density profiles; and neutrino opacities. In Figures 9 – 13, the dependence of neutrino emission on PNS characteristics are shown from the detailed study of Pons et al. (88–90). The generic results (see Figure 9) are that both $L_\nu$ and $< E_\nu >$ increase with increasing mass (85, 88). $< E_\nu >$ for all flavors increases during the first 2-5 seconds of evolution, and then decreases nearly linearly with time. For times larger than about 10 seconds, and prior to the occurrence of neutrino transparency, the $L_\nu$ decays exponentially

with a time constant that is sensitive to the high-density properties of matter. Significant variations in neutrino emission occur beyond 10 seconds: $L_\nu$ is larger during this time for stars with smaller radii and with the inclusion of hyperons in the matter. Finally, significant regions of the stars appear to become convectively unstable during the evolution, as several works have found (95).

The main effect of the larger mean free paths produced by RPA corrections (17, 18, 87) is that the inner core deleptonizes more quickly (see Figure 10). In turn, the maxima in central temperature and entropy are reached on shorter timescales. In addition, the faster increase in thermal pressure in the core slows the compression associated with the deleptonization stage, although after 10 s the net compressions of all models converge. The relatively large, early, changes in the central thermodynamic variables do not, however, translate into similarly large effects on observables such as $L_\nu$ and $< E_\nu >$, relative to the baseline simulation. It is especially important that at and below nuclear density, the corrections due to correlations are relatively small. Since information from the inner core is transmitted only by the neutrinos, the time scale to propagate any high density effect to the neutrinosphere is the neutrino diffusion time scale. Since the neutrinosphere is at a density approximately $0.01 n_0$, and large correlation corrections occur only above $n_0/3$ where nuclei disappear, correlation corrections have an effect at the neutrinosphere only after 1.5 s. However, the corrections are still very important during the longer-term cooling stage (see Figure 11), and result in a more rapid onset of neutrino transparency compared to the Hartree results.

### 5.2.4 Neutrino Signals in Terrestrial Detectors

A comparison of the signals observable with different detectors is shown in Figure 12, which displays $L_\nu$ as a function of baryon mass $M_B$ for stars containing quarks in their cores. In the absence of accretion, $M_B$ remains constant during the evolution, while the gravitational mass $M_G$ decreases. The two upper shaded bands correspond to estimated SN 1987A (50 kpc distance) detection limits with KII and IMB, and the lower bands correspond to estimated detection limits in SNO, SuperK, and UNO, for a Galactic supernova (8.5 kpc distance). The detection limits have been set to a count rate $dN/dt = 0.2$ Hz (89). It is possible that this limit is too conservative and could be lowered with identifiable backgrounds and knowledge of the direction of the signal. The width of the bands represents the uncertainty in $< E_{\bar{\nu}_e} >$ due to the diffusion approximation (88–90). It appears possible to distinguish between stable and metastable stars, since the luminosities when metastability is reached are always above conservative detection limits.

### 5.2.5 Metastable Proto-Neutron Stars

Proto-neutron stars in which strangeness appears following deleptonization can be metastable if their masses are large enough. One interesting diagnostic that could shed light on the internal composition of neutron stars would be the abrupt cessation of the neutrino signal. This would be in contrast to a normal star of similar mass for which the signal continues to fall until it is obscured by the background. In Figure 13 the lifetimes for stars containing hyperons ($npH$), kaons ($npK$) and quarks ($npQ$) are compared (89). In all cases, the larger the mass, the shorter the lifetime. For the kaon and quark PNSs, however, the collapse is delayed until the final stage of the Kelvin-Helmholtz epoch, while this

is not necessarily the case for hyperon-rich stars. In addition, there is a much stronger mass dependence of the lifetimes for the hyperon case.

Clearly, the observation of a single case of metastability, and the determination of the metastability time alone, will not necessarily permit one to distinguish among the various possibilities. Only if the metastability time is less than 10–15 s, could one decide on this basis that the star's composition was that of $npH$ matter. However, as in the case of SN 1987A, independent estimates of $M_B$ might be available (96). In addition, the observation of two or more metastable neutron stars might permit one to differentiate among these models.

## 6 OUTLOOK

On the early universe front, an important issue is simply whether or not light sterile neutrinos exist. If they exist, then the details of light element synthesis could be interestingly different from that of standard Big Bang Nucleosynthesis, because of the neutrino asymmetry amplification phenomenon. One must look forward to crucial experimental results from SNO, MiniBOONe and the long baseline facilities. Naturally, further observational study of the actual light element abundances is a central concern. Precision cosmic microwave background anisotropy measurements will also be important as an independent probe of the baryon to photon ratio, and of the expansion rate of the early universe. An interesting theoretical issue currently under examination is that of inhomogenous neutrino asymmetry creation (97, 98).

The outlook from the supernova perspective hinges on technical advances in handling multigroup, general relativistic, Boltzmann neutrino transport. The advent of next-generation neutrino detectors such as Super-Kamiokande and the

Sudbury Neutrino Observatory promises thousands of neutrino events in the next Galactic supernova. These will provide crucial diagnostics for the supernova mechanism, important limits on the released binding energy and the remnant mass, and critical clues concerning the composition of high density matter. Research in this area will ascertain the extent to which neutrino transport is instrumental in making a supernova explode. Other bonuses include the elucidation of the possible role of supernovae and neutrinos in $r-$process nucleosynthesis.

The main issues that emerge from PNS studies concern the metastability and subsequent collapse to a black hole of a PNS containing quark matter, or other types of matter including hyperons or a Bose condensate, which could be observable in the $\nu$ signal. However, discriminating among various compositions may require more than one such observation. This highlights the need for breakthroughs in lattice simulations of QCD at finite baryon density in order to unambiguously determine the EOS of high density matter. In the meantime, intriguing possible extensions of supernova and PNS simulations with $npQ$ and $npK$ matter include the consideration of heterogenoeus structures and quark matter superfluidity (99).

**Acknowledgements** Research support from DOE grants FG02-88ER-40388 (for MP) and FG02-87ER-40317 and the J.S. Guggenheim Foundation (for JML) is gratefully acknowledged. MP and JML thank Sanjay Reddy, Jose Pons, and Andrew Steiner for benificial collaborations. RFS thanks Adam Burrows for valuable collaborations. His work is supported in part by NSF grant PHY-9900544. RRV would like to thank Nicole Bell, Pasquale Di Bari, Robert Foot, Keith Lee, Mark Thomson and Yvonne Wong for exciting and fruitful collaborations on neu-

trino cosmology. He is supported by the Australian Research Council and the University of Melbourne.

*Literature Cited*

1. Haxton WC 2000. *nucl-th/0004052*
2. Burrows A, 1990. *Ann. Rev. Nucl. Sci.* 40:181–212
3. Hannestad S, Janka H-T, Raffelt G, Sigl G, 2000. *Phys. Rev. D* 62:093021-1–5; Botella FJ, Lim CS, Marciano WJ, 1987. *Phys. Rev. D* 35:896–901
4. McKellar BHJ, Thomson MJ, 1994. *Phys. Rev. D* 49:2710–2728
5. Raffelt G, Sigl G, Stodolsky L, 1993. *Phys. Rev. Lett.* 70:2363–2366
6. Loreti PN, Balantekin AB, 1994. *Phys. Rev. D* 50:4762–4770
7. van Kampen NG, 1992. *Stochastic Processes in Physics and Chemistry* North Holland (Amsterdam) (revised and enlarged edition), ch. XVII
8. Walls DF, Millburn GC, 1994. *Quantum Optics*, Springer (Berlin), ch. 6
9. Bell NF, Sawyer RF, Volkas RR, 2000. *quant-ph/0008133*
10. Lopez RE, Turner MS, 1999. *Phys. Rev. D* 59:103502-1–14
11. Brown LS, Sawyer RF, 2000. *astro-ph/0006370*
12. Sawyer RF, 1975. *Phys. Rev. D* 11:2740–2745
13. Heiselberg H, Pandharipande V, 2000. *Ann. Rev. Nucl. Part. Sci.* 50:481–524
14. Iwamoto N, Pethick CJ, 1982. *Phys. Rev. D* 25:313–329
15. Sawyer RF, 1989. *Phys. Rev. C* 40:865–874
16. Reddy S, Prakash M, Lattimer JM, 1998. *Phys. Rev. D* 58:013009-1–27
17. Reddy S, Prakash M, Lattimer JM, Pons JA, 1999. *Phys. Rev. C* 59:2888–2918
18. Burrows A, Sawyer RF, 1998. *Phys. Rev. C* 58:554–571
19. Bäckmann SO, Brown GE, Niskanen JA, 1985. *Phys. Rep.* 124:1-68
20. Horowitz CJ, Wehrberger K, 1991. *Nucl. Phys. A* 531: 665–684; 1991. *Phys. Rev. Lett.* 66: 272–275; 1991. *Phys. Lett. B* 266:236–242
21. Freedman DZ, 1974. *Phys. Rev. D* 9: 1389–1392
22. Lattimer JM, Burrows A, 1991. In SN 1987A and Other Supernovae, ed. I. J. Danziger

and K. Kjar (European Southern Observatory, Garching bei Munchen), pp. 69–81

23. Reddy S, Bertsch GF, Prakash M, 2000. *Phys. Lett. B* 475:1–8
24. Horowitz CJ 1997. *Phys. Rev. D* 55:4577–45
25. Prakash M, Bombaci I, Prakash Manju, Ellis PJ, Lattimer JM, Knorren R, 1997. *Phys. Rep.* 280:1–77; Ellis PJ, Lattimer JM, Prakash M, 1996. *Comm. Nucl. Part. Phys.* 22:63–75; Prakash M, Cooke JR, Lattimer JM, 1995. *Phys. Rev. D* 52:661–665; Steiner AW, Prakash M, Lattimer JM, 2000. *Phys. Lett.* B486:239–248
26. Lattimer JM, Pethick CJ, Prakash M, Haensel P, 1991. *Phys. Rev. Lett.* 66:2701–2704
27. Glendenning NK, 1992. *Phys. Rev. Lett.* 46:1274–1287
28. Steiner AW, Prakash M, Lattimer JM, 2001. *astro-ph/0101566*
29. Glendenning NK, Pei S, 1995. *Phys. Rev. C* 52:2250–2253 Glendenning NK, Schaffner-Bielich J, 1998. *Phys. Rev. Lett.* 81:4564–4567; *Phys. Rev. C* 60: 025803-1–13; Christiansen MB, Glendenning NK, Schaffner-Bielich J, 2000. *Phys. Rev. C* 62:025804-1–6; Norsen T, Reddy S, 2000. *nucl-th/0010075*
30. Kolb EW, Turner MS, 1990. *The Early Universe*, Addison-Wesley, ch. 4.
31. Harris RA, Stodolsky L, 1978. *Phys. Lett. B* 78:313–317
32. Harris RA, Stodolsky L, 1982. *Phys. Lett. B* 116:464–468
33. Dolgov A, 1981. *Sov. J. Nucl. Phys.* 33:700–706
34. Stodolsky L, 1987. *Phys. Rev. D* 36:2273–2277
35. Thomson M, 1991. *Phys. Rev. A* 45:2243–2249
36. Enqvist K, Kainulainen K, Maalampi J, 1991. *Nucl. Phys. B* 349:754–790
37. Foot R, Lew H, Volkas RR, 1992. *Mod. Phys. Lett. A* 7:2567–2574
38. Foot R, 1994. *Mod. Phys. Lett. A* 9:169–180
39. Foot R, Volkas RR, 1995. *Phys. Rev. D* 52:6595–6606
40. Foot R, Volkas RR, 2000. *Phys. Rev. D* 61:043507-1–34
41. Foot R, Thomson MJ, Volkas RR, 1996. *Phys. Rev. D* 53:5349–5353
42. Foot R, Volkas RR, 1997. *Phys. Rev. D* 56:6653–6664; 59:029901(E)
43. Affleck I, Dine M, 1985. *Nucl. Phys. B* 249:361–380
44. Casas JA, Cheng WY, Gelmini GB, 1999. *Nucl. Phys. B* 538:297–308
45. Wolfenstein L, 1978. *Phys. Rev. D* 17:2369–2374

46. Mikheyev SP, Smirnov AYu, 1986. *Nuovo Cimento C* 9:17–26
47. Nötzold D, Raffelt G, 1988. *Nucl. Phys. B* 307:924–936
48. Foot R, Volkas RR, 1997. *Phys. Rev. D* 55:5147–5176
49. Foot R, 1999. *Astropart. Phys.* 10:253–273
50. Di Bari P, Foot R, 2000. *Phys. Rev. D* 61:105012-1–14
51. Shi X, 1996. *Phys. Rev. D* 54:2753–2760
52. Enqvist K, Kainulainen K, Sorri A, 1999. *Phys. Lett. B* 464:199–205
53. Braad P-E, Hannestad S, 2000. *hep-ph/0012194*
54. Buras R, 2000. *hep-ph/0002086*
55. Kirilova DP, Chizhov MV, 1997. *Phys. Lett. B* 393:375–382
56. Bell NF, Volkas RR, Wong YYY, 1999. *Phys. Rev. D* 59:113001-1–22
57. Kirilova DP, Chizhov MV, 1998. *Phys. Rev. D* 58:073004-1–14; *Nucl. Phys. B* 534:447–463
58. Kirilova DP, Chizhov MV, 2000. *Nucl. Phys. B* 591:457–468
59. Volkas RR, Wong YYY, 2000. *Phys. Rev. D* 62:093024-1–19
60. Lee KSM, Volkas RR, Wong YYY, 2000. *Phys. Rev. D* 62:093025-1–7
61. Bell NF, Foot R, Volkas RR, 1998. *Phys. Rev. D* 58:105101-1–6
62. Dolgov A, Hansen SH, Pastor S, Semikoz DV, 2000. *Astropart. Phys.* 14:79–90
63. Di Bari P, Foot R, Volkas RR, Wong YYY, 2000. *hep-ph/0008245*, *Astropart. Phys.* (in press)
64. Sorri A, 2000. *Phys. Lett. B* 477:201–207
65. Buras R, Semikoz DV, 2000. *hep-ph/0008263*
66. Barbieri R, Dolgov A, 1990. *Phys. Lett. B* 237:440–445
67. Barbieri R, Dolgov A, 1991. *Nucl. Phys. B* 349:743–753
68. Kainulainen K, 1990. *Phys. Lett. B* 244:191–195
69. Enqvist K, Kainulainen K, Thomson M, 1992. *Nucl. Phys. B* 373:498–528
70. Cline J, 1992. *Phys. Rev. Lett.* 68:3137–3140
71. Shi X, Schramm DN, Fields, BD, 1993. *Phys. Rev. D* 48:2563–2572
72. Di Bari P, Lipari P, Lusignoli M, 2000. *Int. J. Mod. Phys. A* 15:2289–2328
73. Shi X, Fuller GM, 1999. *Phys. Rev. D* 59:063006-1–8
74. Foot R, 1999. *Phys. Rev. D* 61:023516-1–14

75. Lange AE et al 2001. *Phys. Rev. D* 63:042001-1–8
76. Balbi A et al 2000. *Astrophys. J.* 545:L1–4
77. Di Bari P, Foot R, 2000. *Phys. Rev. D* 63L043008-1–9
78. Bell NF, Sawyer RF, Volkas RR, 2001. *Phys. Lett. B* 500:16–21
79. Colgate SA, White RH, 1966. *Astrophys. J.* 143:626–681
80. Bethe HA, Brown GE, Applegate J, Lattimer JM, 1979. *Nucl. Phys.* A324:487–533
81. Burrows A, Goshy J, 1993. *Astrophys. J.* 416:L75–78
82. Burrows A 2000. *Nature* 403:727–733
83. O.E.B. Messer, A. Mezzacappa, S.W. Bruenn, and M.W. Guidry, 1998. *Astrophys. J.* 507:353–360; Yamada S, Janka H-Th, Suzuki H, 1999. *Astron. Astrophys.* 344:533–550; Burrows A, Young T, Pinto P, Eastman R, Thompson TA, 2000. *Astrophys. J.* 539:865–887; Rampp M, Janka H-Th, 2000. *Astrophys. J.* 539:L33–36; Liebendoerfer M, *et al.* 2000. *astro-ph/0006418*
84. Thompson TA, Burrows A, Horvath JE, 2000. *Phys. Rev. C* 62:035802-1–18
85. Burrows A, Lattimer JM, 1986. *Astrophys. J.* 307:178–196
86. Keil W, Janka H-T, 1995. *Astron. & Astrophys.* 29:145–163
87. Burrows A, Sawyer, RF, 1999. *Phys. Rev. C* 59:510–514
88. Pons JA, Reddy S, Prakash M, Lattimer JM, Miralles JA, 1999. *Astrophys. J.* 513:780–804
89. Pons JA, Miralles JA, Prakash M, Lattimer JM, 2001. *astro-ph/0008389*, *Astrophys. J.*, in press
90. Pons JA, Steiner AW, Prakash M, Lattimer JM, 2001. *astro-ph/0102015*, *Phys. Rev. Lett.*, submitted;
91. Jung CK, 2000. In *Next Generation Nucleon Decay and Neutrino Dectector*, ed. by Diwan N, Jung CK (AIP New York), 29–34
92. Burrows A, 1988. *Astrophys. J.* 334:891–908
93. Lindquist RW, 1966. *Ann. Phys.* 37:478–518
94. Thorne KS, 1981. *Mon. Not. R. Astron. Soc.* 194:439–473
95. Burrows A, Fryxell B, 1993. *Astrophys. J. Lett.* 418:L33–35; Herant M, Benz W, Hicks J, Fryer C, Colgate SA, 1994. *Astrophys. J.* 435:339–361; Keil W, Janka H-T, Müller E, 1995. *Astrophys. J. Lett.* 473:L111–114; Mezzacappa A, Calder AC, Bruenn SW, Blondin JM,

Guidry MW, Strayer MR, Umar AS, 1998. *Astrophys. J.* 495:911–926; Miralles JA, Pons JA, Urpin VA, 2000. *Astrophys. J.* 543:1001–1006

96. Thielemann FK, M. Hashimoto M, Nomoto K, 1990. *Astrophys. J.* 349:222-240; Bethe HA, Brown GE, 1995. *Astrophys. J. Lett.* 445:L129–132
97. Di Bari P 2000, *Phys. Lett.* B482:150-160
98. Enqvist K, Kainulainen K, Sorri A 2000, hep-ph/0012291
99. Carter GW, Reddy S, 2000. *Phys. Rev. D* 62:103002-1–9

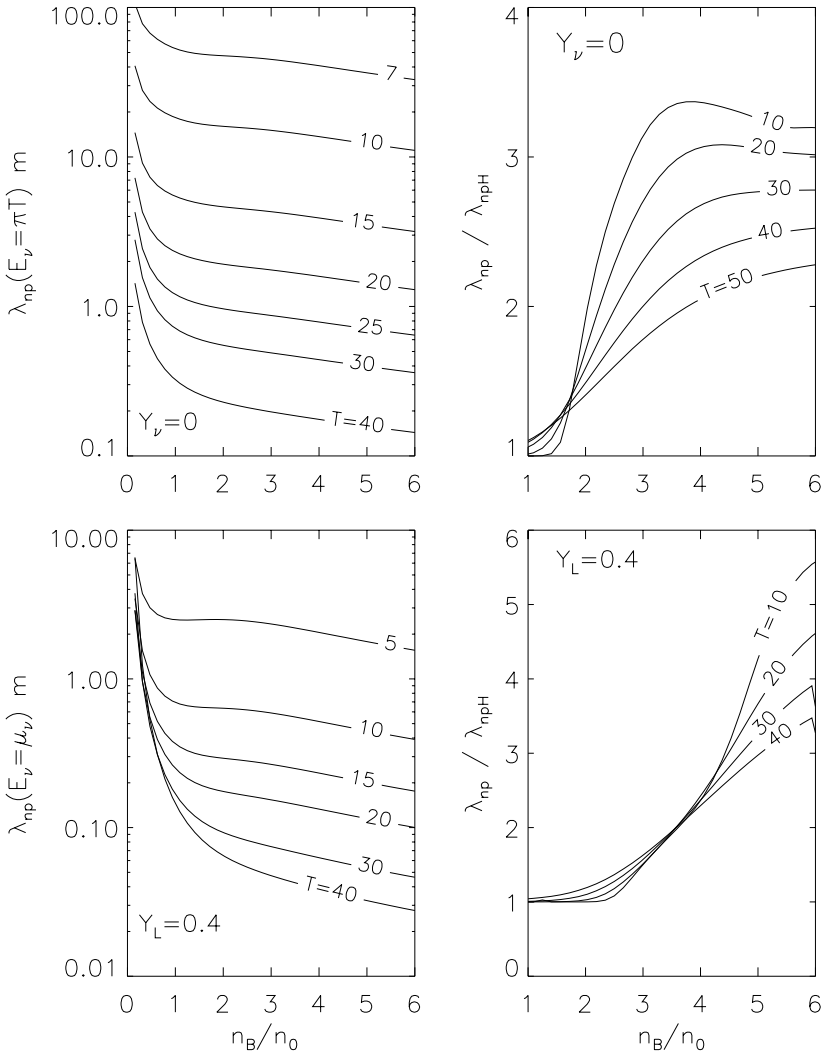


Figure 1: Neutrino mean free paths in matter with nucleons only (left panels). Right panels show ratios of mean free paths in matter without and with hyperons. Top panels show scattering mean free paths (common to all neutrino species). Bottom panels show $\nu_e$ mean free paths including absorption reactions. The figure is from Ref. (16).

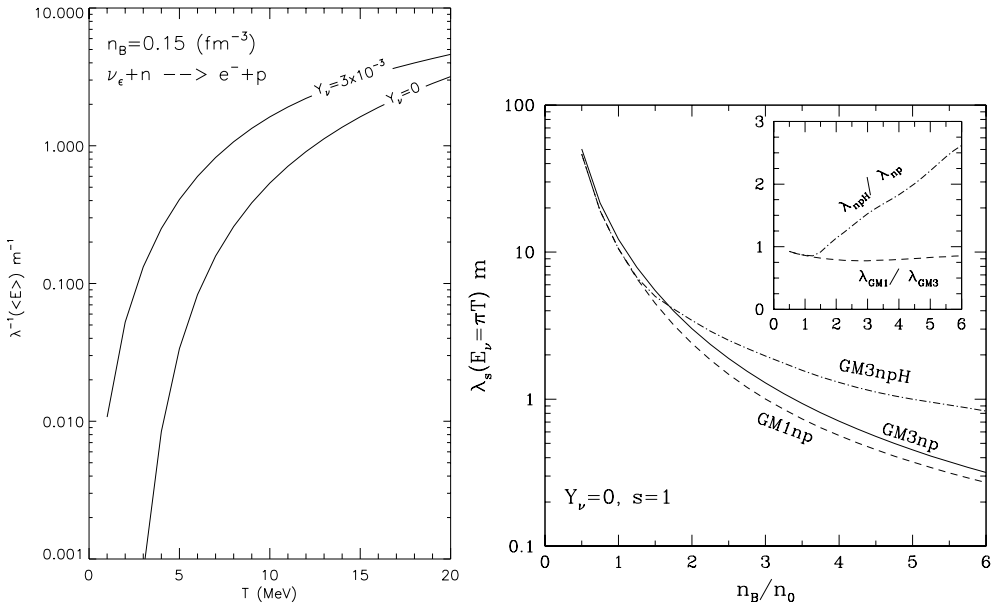


Figure 2: Left: Charged current inverse neutrino mean free paths. Right: Comparison of scattering mean free paths in neutrino poor matter at fixed entropy in matter containing nucleons and also hyperons. The figure is from Ref. (16).

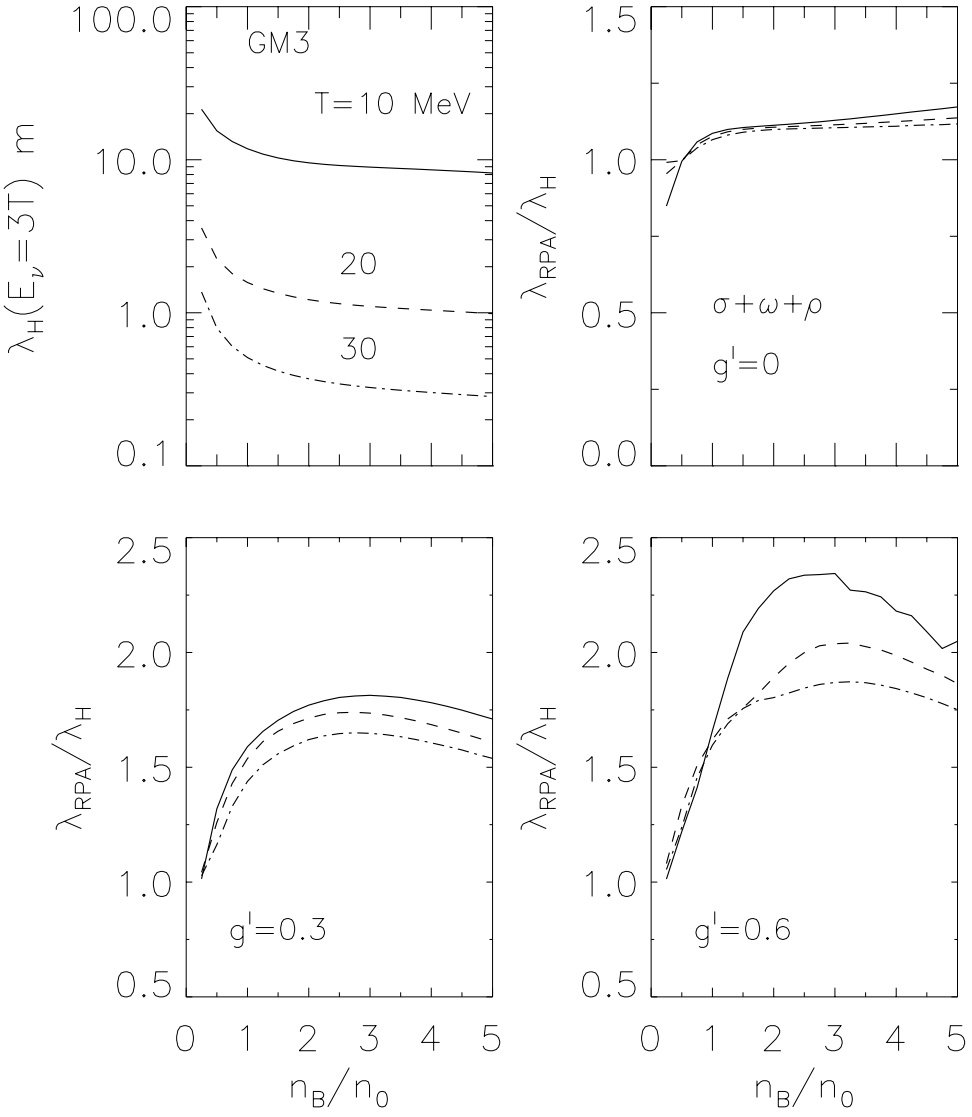


Figure 3: The density and temperature dependences of the neutral current mean free paths for neutrino free matter in the field-theoretical model GM3. The upper left panel shows the Hartree results for the case $E_\nu = 3T$. The influence of the spin correlations introduced via the Migdal parameter $g'$ is strong, as can be deduced from the results shown in the upper right and bottom panels. The figure is from Ref. (17).

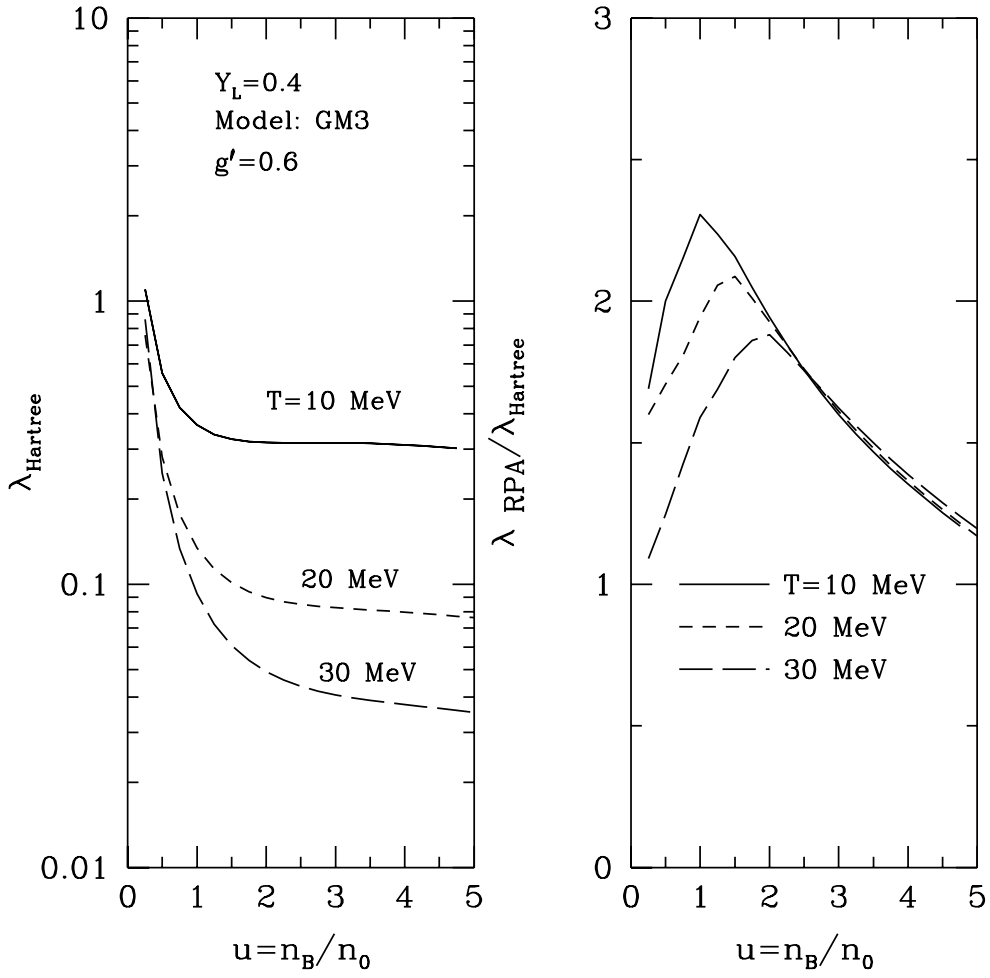


Figure 4: The density and temperature dependences of the charged current neutrino mean free path in $\beta-$stable matter for the GM3 model assuming $Y_L = 0.4$. Results for the Hartree approximation (left panel) are compared with those including RPA corrections (right panel) with $g' = 0.6$. The figure is from Ref. (17).

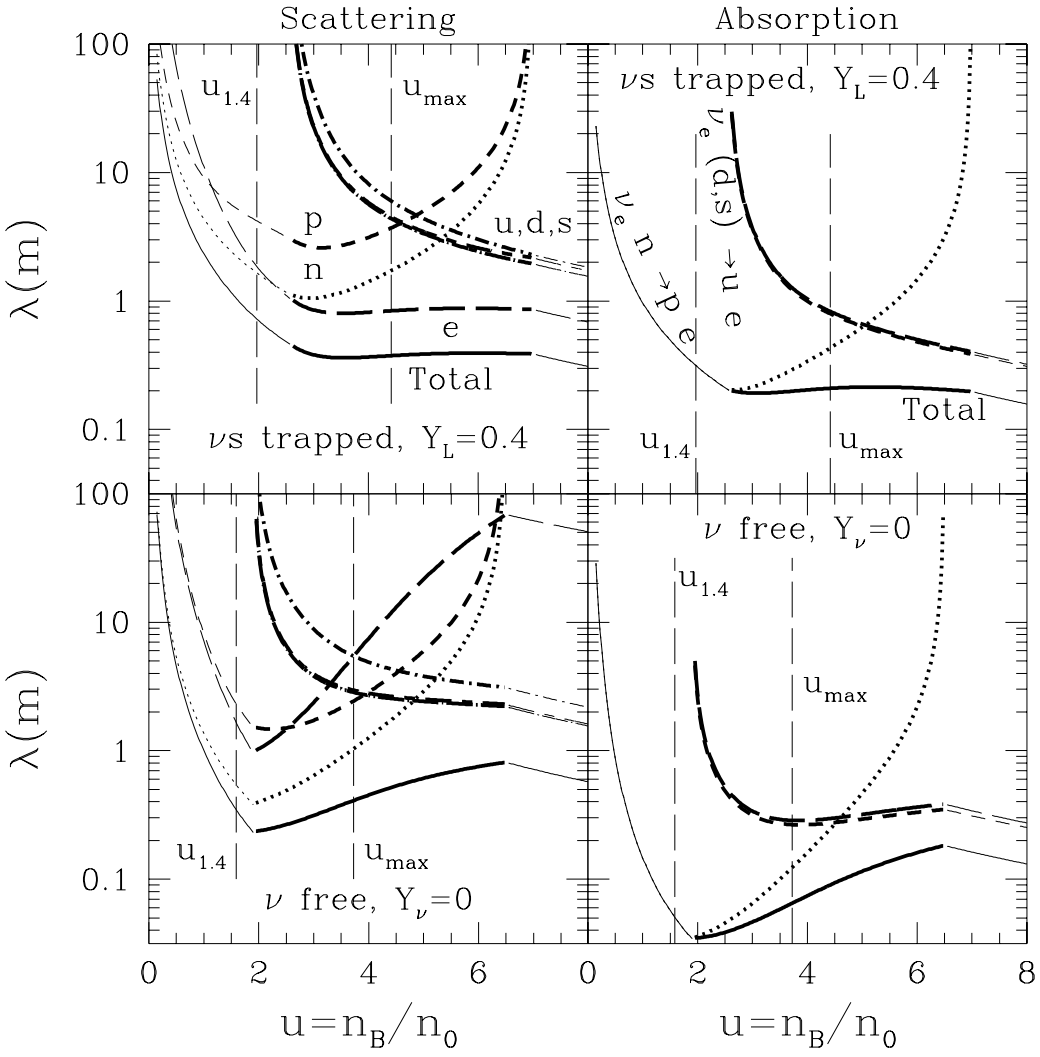


Figure 5: $\nu_e$ mean free paths from various particles in matter containing a mixed phase of quarks and hadrons. Thick lines show the extent of the mixed phase region. Left (right) panels show scattering (absorption) mean free paths. The upper (lower) panels correspond to the neutrino-trapped (neutrino-free) era. Vertical dashed lines labelled $u_{1.4}$ and $u_{max}$ indicate the central densities of 1.4 $M_\odot$ and maximum mass (2.22 $M_\odot$ for the upper panels and 1.89 $M_\odot$ for the lower panels) stars, respectively.

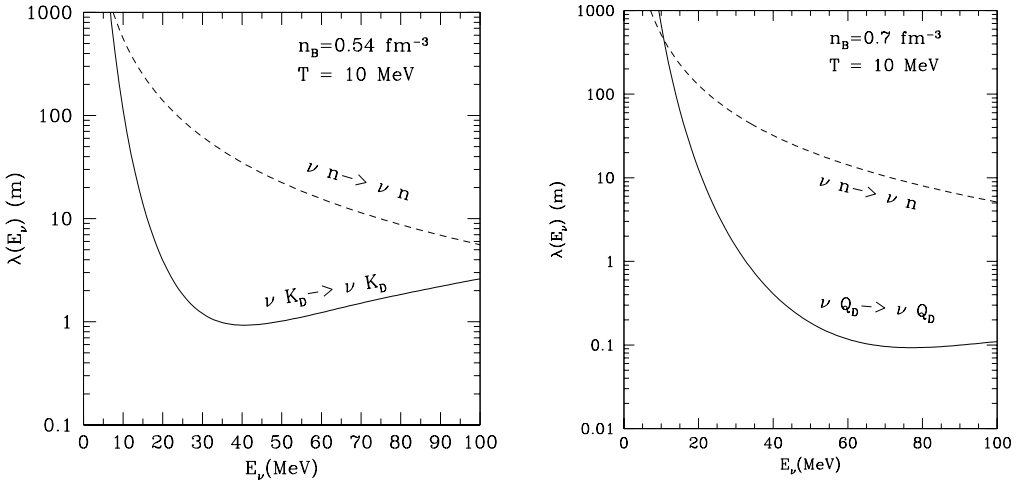


Figure 6: Transport neutrino mean free paths in heterogeneous media. Solid lines are for matter in a mixed phase containing kaons (left panel) and quarks (right panel), and dashed curves are for uniform matter. This figure is from Ref. (23).

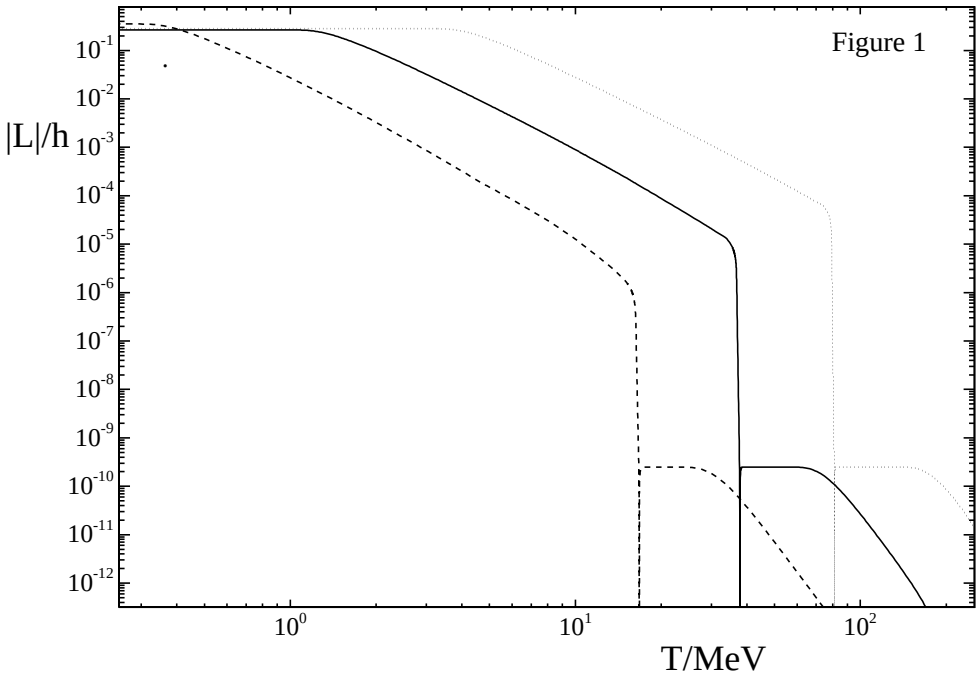


Figure 7: Neutrino asymmetry growth curves driven by $\nu_\tau \leftrightarrow \nu_s$ and $\overline{\nu}_\tau \leftrightarrow \overline{\nu}_s$ oscillations. The mixing angle is selected to be $\sin^2 2\theta_0 = 10^{-8}$. The three curves correspond to $\Delta m^2 = -0.5$, $-50$ and $-5000$ eV$^2$, reading from left to right. This figure is taken from Ref. (49).

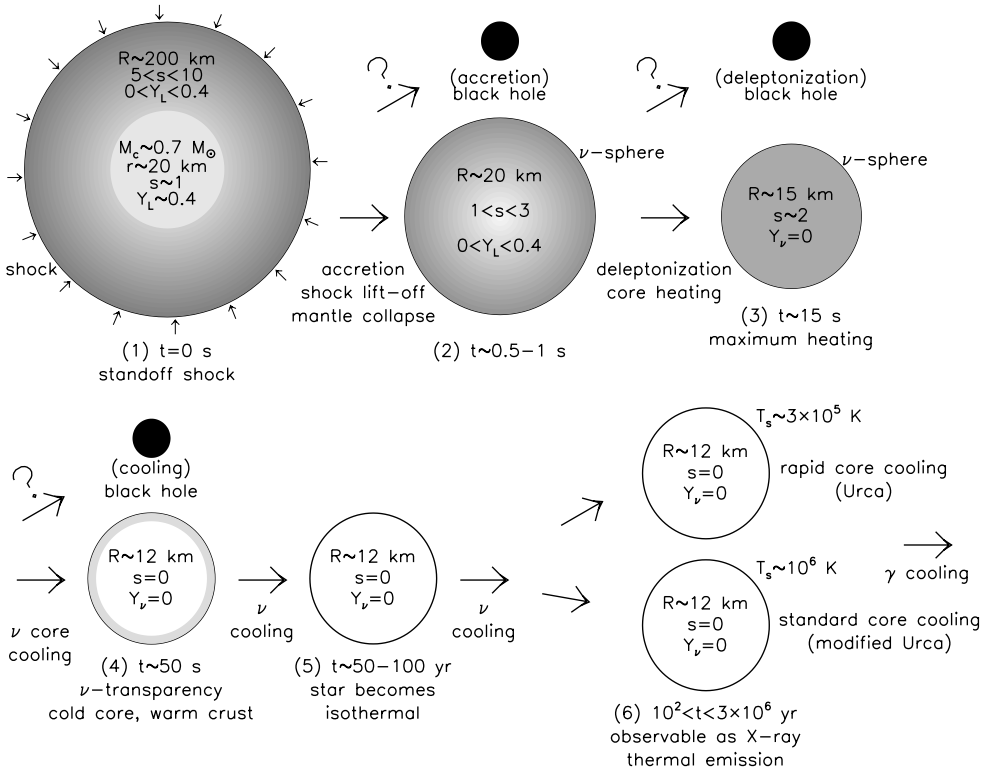


Figure 8: The main stages of evolution of a neutron star. Shading indicates, approximately, relative temperatures. This figure is from Ref. (25).

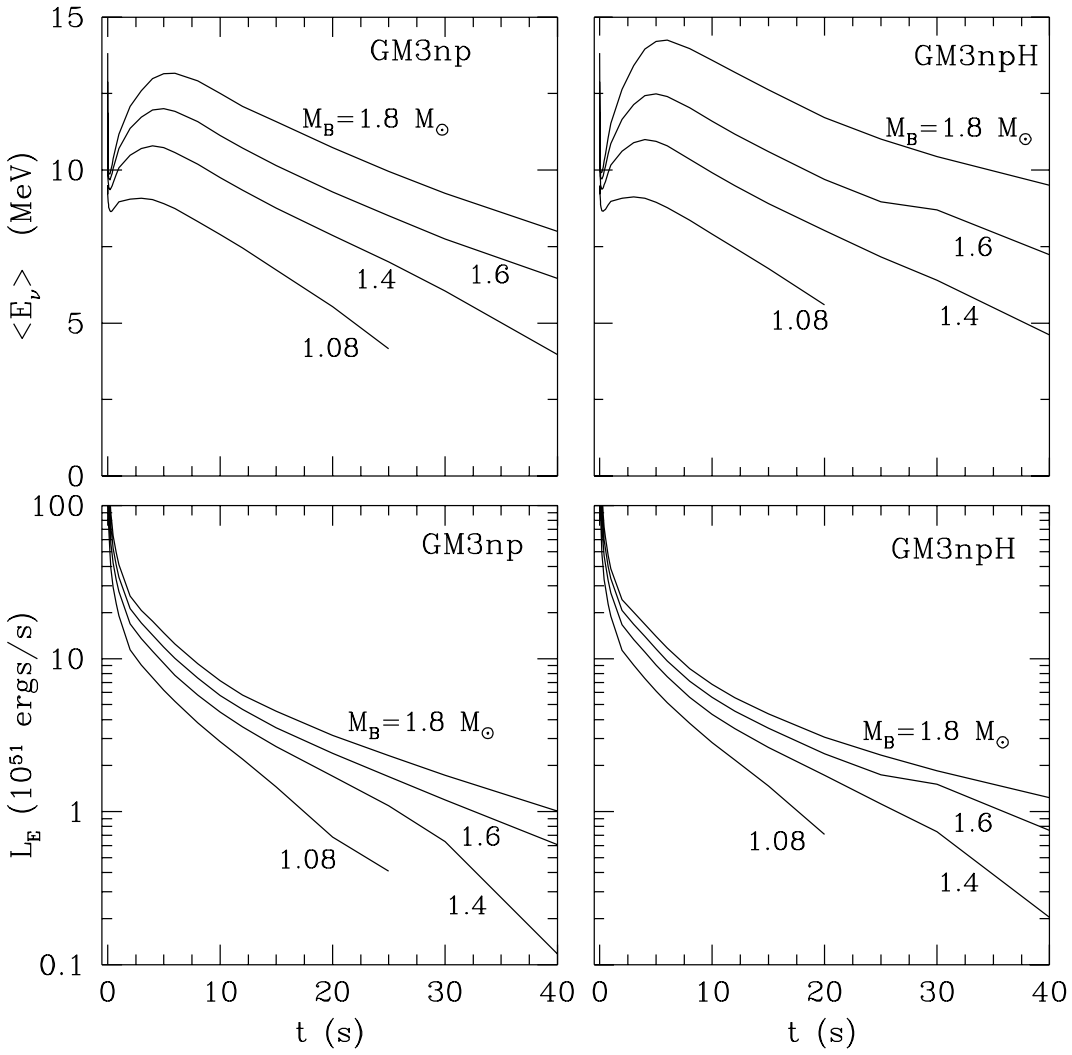


Figure 9: The evolution of the average energy and total luminosity of neutrinos in PNSs composed of baryons only (left panel) and baryons and hyperons (right panel). The figure is from Ref. (88).

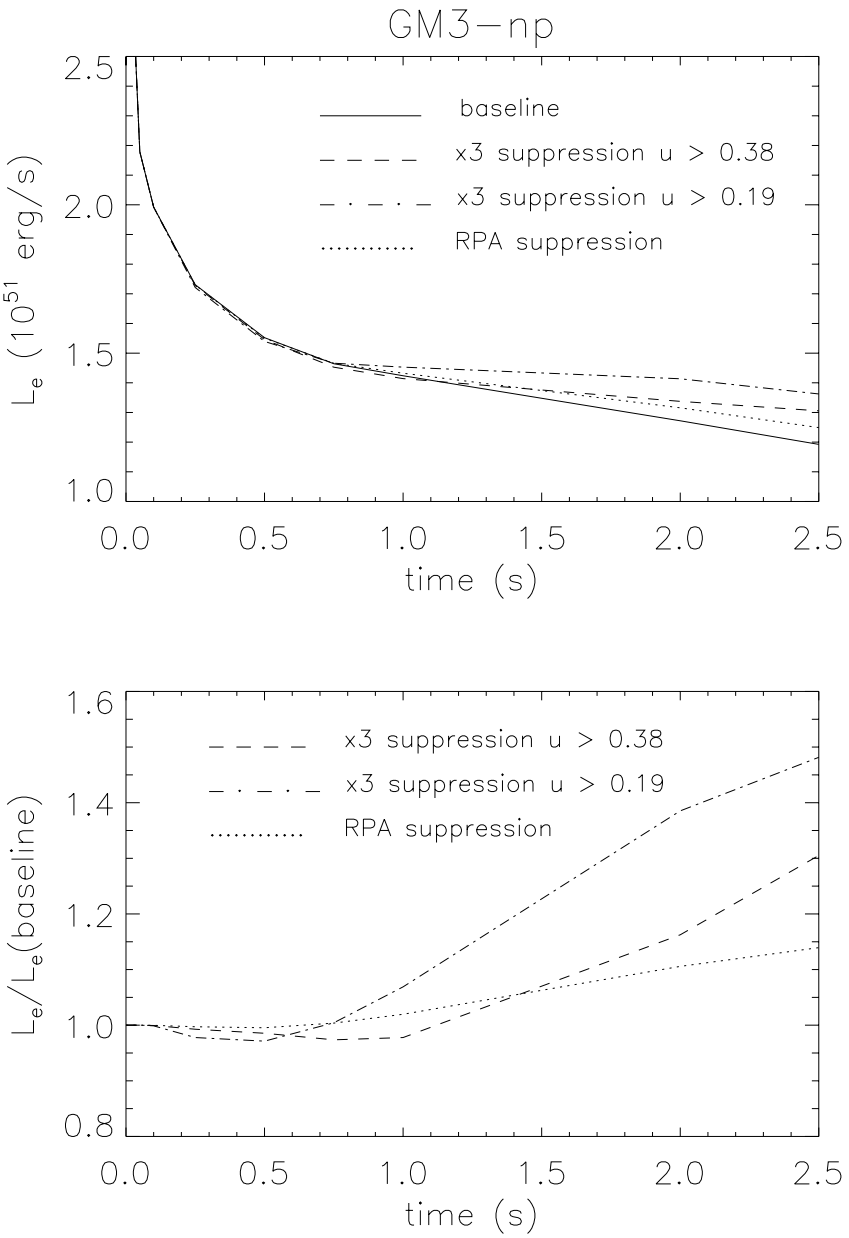


Figure 10: The upper panel shows the total emitted neutrino luminosity for the evolution of a PNS using the opacities of Ref. (17). Here $u = n_B/n_0$. The lower panel shows the ratio of the luminosities obtained for models with correlation corrections to the baseline (Hartree approximation) model. This figure is from Ref. (88).

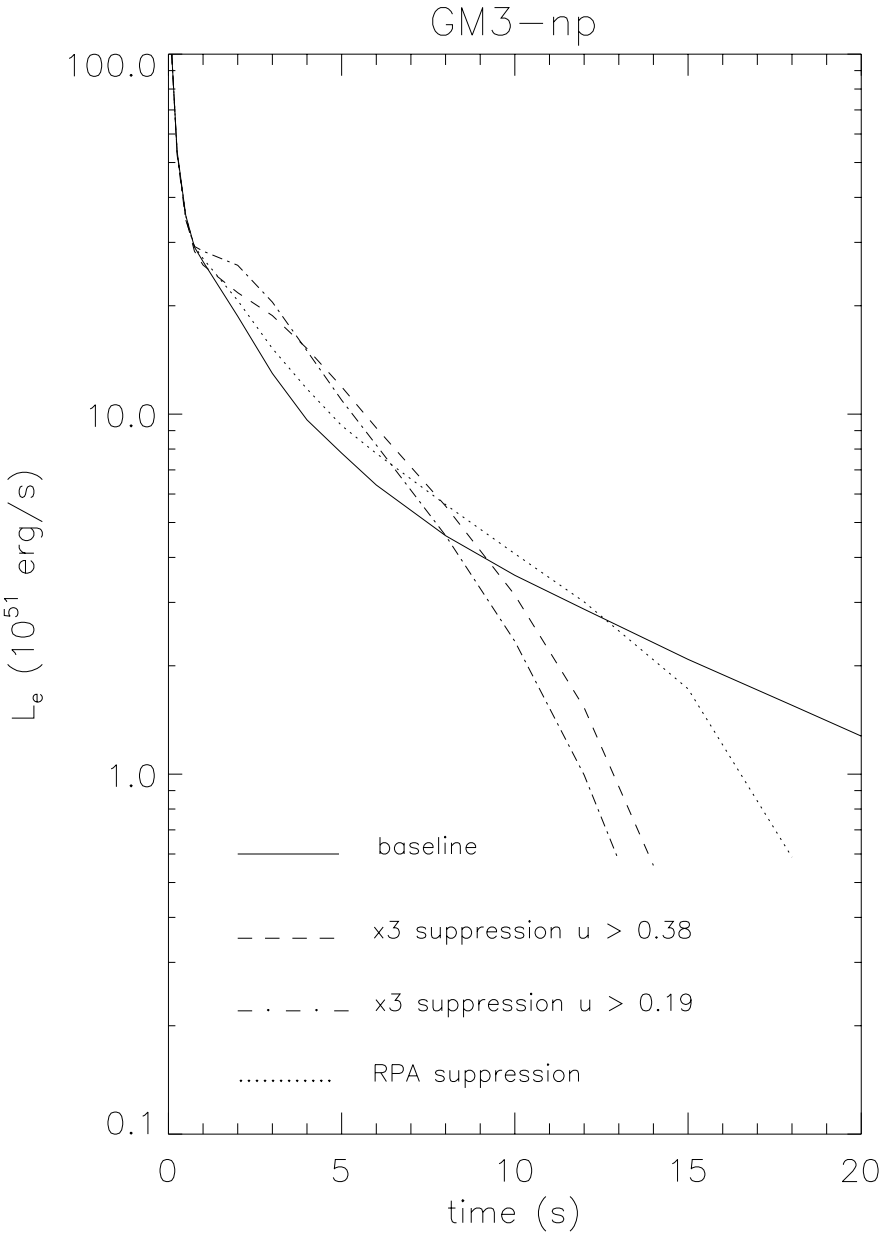


Figure 11: Emitted neutrino luminosity in PNSs ($u = n_B/n_0$). This figure is from Ref. (88).

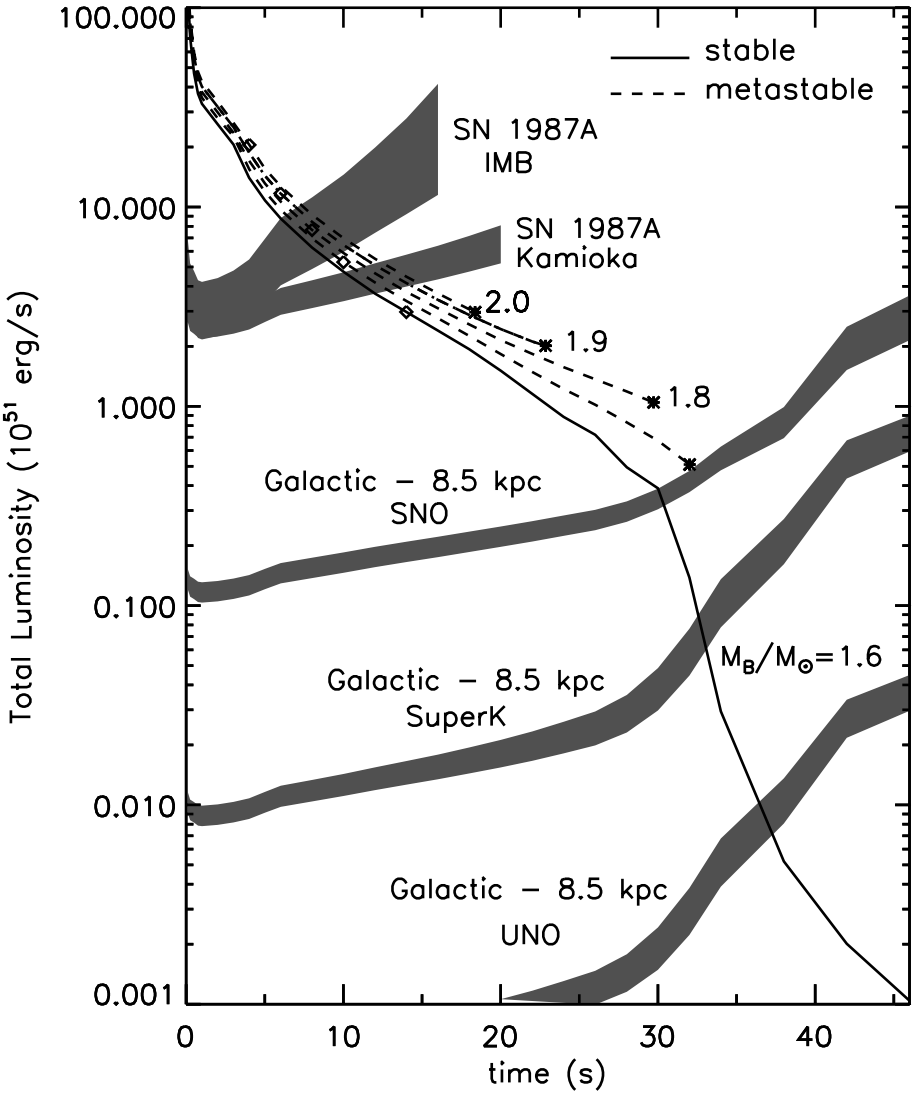


Figure 12: The evolution of the total neutrino luminosity for *npQ* PNSs. Shaded bands illustrate the limiting luminosities corresponding to a count rate of 0.2 Hz, assuming a supernova distance of 50 kpc for IMB and Kamioka, and 8.5 kpc for SNO and SuperK. The widths of the shaded regions represent uncertainties in the average neutrino energy from the use of a diffusion scheme for neutrino transport. This figure is from Ref. (90).

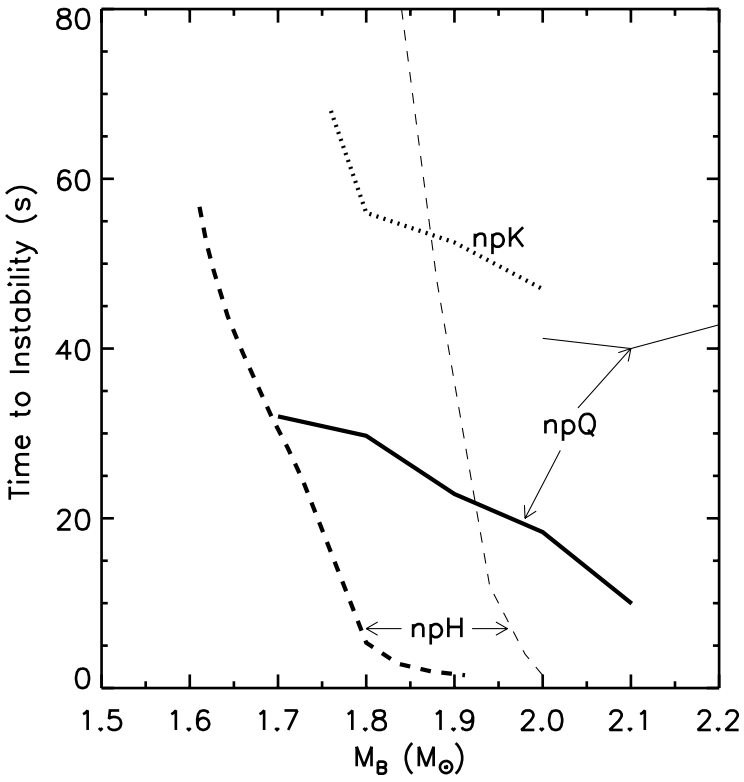


Figure 13: Lifetimes of metastable stars versus the PNS baryon mass $M_B$. Thick lines denote cases in which the maximum gravitational masses of cold, catalyzed stars are near 1.45 $M_\odot$, which minimizes the metastability lifetimes. The thin lines for the *npQ* and *npH* cases are for EOSs with larger maximum gravitational masses (1.85 and 1.55 $M_\odot$, respectively.) This figure is from Ref. (90).

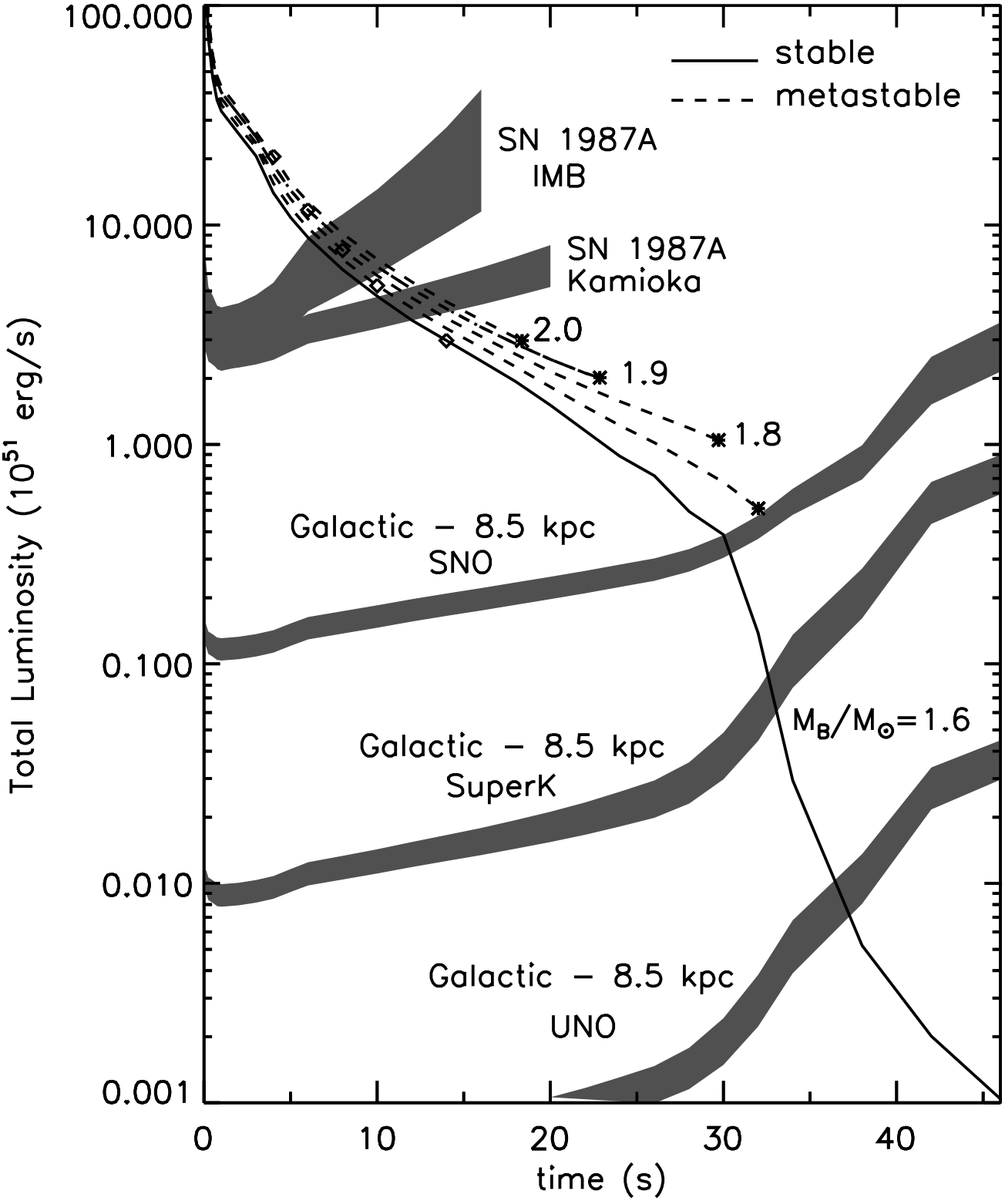
100.000
10.000
1.000
0.100
0.010
0.001
Total Luminosity ($10^{51}$ erg/s)
0
10
20
30
40
time (s)
stable
metastable
SN 1987A
IMB
SN 1987A
Kamioka
2.0
1.9
1.8
Galactic – 8.5 kpc
SNO
Galactic – 8.5 kpc
SuperK
Galactic – 8.5 kpc
UNO
$M_B/M_\odot$=1.6

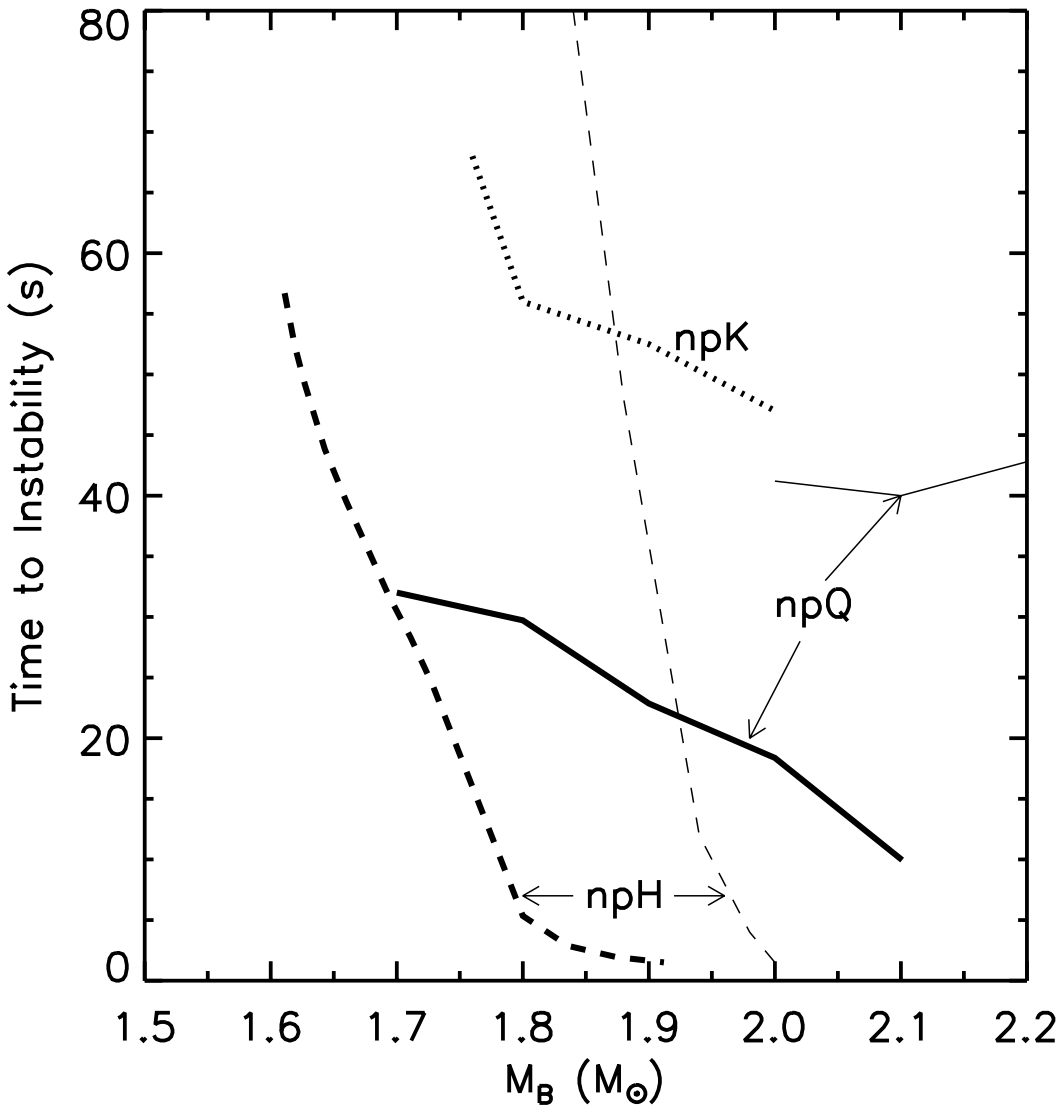
80
60
40
20
0
Time to Instability (s)
1.5
1.6
1.7
1.8
1.9
2.0
2.1
2.2
$M_B$ ($M_\odot$)
npK
npQ
npH